THE ASTROPHYSICAL JOURNAL, 315:621–645, 1987 April 15

MOLECULAR ABUNDANCES IN OMC-1: THE CHEMICAL COMPOSITION OF INTERSTELLAR MOLECULAR CLOUDS AND THE INFLUENCE OF MASSIVE STAR FORMATION

GEOFFREY A. BLAKE
Department of Physics and Department of Chemistry, University of California, Berkeley, and Department of Physics, California Institute of Technology

E. C. SUTTON
Department of Physics and Space Sciences Laboratory, University of California, Berkeley

AND

C. R. MASSON AND T. G. PHILLIPS
Department of Physics, California Institute of Technology
Received 1986 August 8; accepted 1986 October 1

ABSTRACT

We present here an investigation of the chemical composition of the various regions in the core of the Orion molecular cloud (OMC-1) based on results from the Caltech Owens Valley Radio Observatory (OVRO) millimeter-wave spectral line survey (Sutton *et al.*; Blake *et al.*). This survey covered a 55 GHz interval in the 1.3 mm (230 GHz) atmospheric window and contained emission from over 800 resolved spectral features. Of the 29 identified species 14 have a sufficient number of detected transitions to be investigated with an LTE "rotation diagram" technique, in which large numbers of lines are used to estimate both the rotational excitation and the overall abundance. The rotational temperatures and column densities resulting from these fits have then been used to model the emission from those remaining species which either have too few lines or which are too weak to be so analyzed. When different kinematic sources of emission are blended to produce a single feature, Gaussian fits have been used to derive the individual contributions to the total line profile. The uniformly calibrated data in the unique and extensive Caltech spectral line survey lead to accurate estimates of the chemical and physical parameters of the Orion molecular cloud, and place significant constraints on models of interstellar chemistry.

A global analysis of the observed abundances shows that the markedly different chemical compositions of the kinematically and spatially distinct Orion subsources may be interpreted in the framework of an evolving, initially quiescent, gas-phase chemistry influenced by the process of massive star formation. The chemical composition of the extended Orion cloud complex is similar to that found in a number of other objects, but the central regions of OMC-1 have had their chemistry selectively altered by the radiation and high-velocity outflow from the young stars embedded deep within the interior of the molecular cloud. Specifically, the extended ridge clouds are inferred to have a low (subsolar) gas-phase oxygen content from the prevalence of reactive carbon-rich species like CN, CCH, and C_3H_2 also found in more truly quiescent objects such as TMC-1. The similar abundances of these and other simple species in clouds like OMC-1, Sgr B2, and TMC-1 lend support to gas-phase ion-molecule models of interstellar chemistry, but grain processes may also play a significant role in maintaining the overall chemical balance in such regions through selective depletion mechanisms and grain mantle processing. In contrast, the chemical compositions of the more turbulent plateau and hot core components of OMC-1 are dominated by high-temperature, shock-induced gas and grain surface neutral-neutral reaction processes. The high silicon/sulfur oxide and water content of the plateau gas is best modeled by fast shock disruption of smaller grain cores to release the more refractory elements followed by a predominantly neutral chemistry in the cooling postshock regions, while a more passive release of grain mantle products driven toward kinetic equilibrium most naturally explains the prominence of fully hydrogenated N-containing species like HCN, NH_3, CH_3CN, and C_2H_5CN in the hot core. The clumpy nature of the outflow is illustrated by the high-velocity emission observed from easily decomposed molecules such as H_2CO. Areas immediately adjacent to the shocked core in which the cooler, ion-rich gas of the surrounding molecular cloud is mixed with water/oxygen rich gas from the plateau source are proposed to give rise to the enhanced abundances of complex internal rotors such as CH_3OH, $HCOOCH_3$, and CH_3OCH_3 whose line widths are similar to carbon-rich species such as CN and CCH found in the extended ridge, but whose rotational temperatures are somewhat higher and whose spatial extents are much more compact.

Subject headings: interstellar: abundances — interstellar: molecules — molecular processes — stars: formation

I. INTRODUCTION

As compared with the lengthy history of traditional astronomical observations, the study of interstellar molecules, and thereby interstellar chemistry, is still in its infancy. While much has been learned about stellar structure, evolution, and chemistry, considerably less is known about the interstellar matter from which stars form and to which they return mass at the end of their lives. The interplay of matter between stars and the

interstellar medium is a complex process, but its investigation is vital to our complete understanding of the structure and dynamics of galaxies, including our own. As matter is cycled between stellar interiors and the interstellar gas, its chemical composition is affected by both environments, and besides being of interest in its own right, the characterization of interstellar chemistry will therefore eventually lead to a more comprehensive analysis of galactic composition and evolution. In addition, the exotic conditions prevailing in the interstellar medium have made it possible to examine fundamental chemical and physical processes such as the formation and destruction of molecules at pressures, temperatures, and time scales that would be impossible to reproduce in the laboratory.

The rapid advances in radio and millimeter-wave technology in the 23 years since the discovery of the interstellar OH lambda doublets have revolutionized our concepts about the nature of the neutral gas in our Galaxy. Astronomical observations at these wavelengths have revealed an entirely new type of object, the so-called dense molecular cloud, in which over 60 atomic and molecular species have now been identified—a richness and complexity totally unexpected even a decade ago. Because the gas and dust in "typical" molecular clouds have temperatures on the order of 10–100 K, the bulk of the radiation emitted by such objects lies at millimeter (10–1 mm), submillimeter (1–0.1 mm), and far-infrared (100–30 μm) (FIR) wavelengths where the interaction of electromagnetic radiation with the rotational motion of simple molecules is at a maximum and where attenuation by interstellar dust is negligible. It is for these reasons that most interstellar molecules have been detected using rotational spectroscopic methods in the microwave region. Observations at higher frequencies are more difficult but are equally important because the pure rotational transitions of molecular hydrides and the fine-structure transitions of low-Z atoms lie exclusively at submillimeter or far-infrared wavelengths. Spectral lines in the relatively unexplored region above 200 GHz can therefore be quite informative because they provide powerful, and often unique, probes into the chemical and physical nature of the interstellar gas. In addition to producing some of the most accurate estimates of the chemical abundances, temperatures, and densities within molecular clouds, near millimeter-wave spectral lines also contribute substantially to the energy balance in these objects and are therefore important in their own right. The amount of energy lost from rotational emission lines determines, in part, the rates of collapse and ultimately the efficiency of star formation in molecular clouds, and is very sensitive to the exact chemical composition of the gas.

Whereas previously only isolated observations of selected species were possible, the improved performance of new large-aperture telescopes and low-noise broad-band receivers has recently allowed unbiased millimeter-wave surveys of molecular line emission to be conducted on a number of objects (Johansson *et al.* 1984; Cummins, Linke, and Thaddeus 1986). The most extensive spectral line survey of this type is that of the Orion molecular cloud (OMC-1) conducted at the Caltech Owens Valley Radio Observatory (OVRO) (Sutton *et al.* 1985; Blake *et al.* 1986). The great strength and number density of rotational emission lines from OMC-1 near 1.3 mm is dramatically illustrated in the compressed view of the Caltech spectral line survey presented in Figure 1. This figure shows that the millimeter-wave spectra of molecular clouds can become as dense as those of stellar atmospheres, and that the sensitivity is now sufficient to begin a comprehensive investigation of the broad-band spectral properties of molecular clouds. In fact, large portions of the Caltech survey are "confusion-limited" in that rotational emission lines stronger than the anticipated noise level occupy the entire passband. The combined flux in emission lines is a major fraction of the energy output at millimeter wavelengths in OMC-1 (Sutton *et al.* 1984). The examination of large parts of the millimeter-wave spectrum has several advantages over isolated, single line measurements. These include a more secure identification of new interstellar species, more accurate estimates of the temperatures and densities of molecular clouds, a more complete sampling of the chemical composition of the interstellar medium, and a separation of the total radiative output of molecular clouds into its true continuum component and that due to integrated molecular line emission.

We have previously presented a detailed description of the lines detected in the Caltech survey along with a preliminary account of the physical and chemical conditions prevailing in OMC-1 as determined by its millimeter-wave spectrum (Sutton *et al.* 1985; Blake *et al.* 1986). Here we discuss in greater detail the overall physical condition and chemical composition of the Orion molecular cloud, concentrating in particular on the observable effects of massive star formation in the cloud core. The unique spectral signatures of the various emission components in OMC-1 allow the chemical and physical composition of each region to be analyzed separately, in this case using a simple LTE "rotation diagram" technique. After decomposing the emission into its component parts and constructing estimates of the various source parameters, we then present a discussion of the processes expected to determine the chemical compositions of active molecular clouds and compare the predictions of models incorporating such processes with the observationally determined molecular abundances. The nature of OMC-1 is sufficiently complex that a brief description of its physical structure is warranted before beginning a detailed discussion of the spectral line survey.

II. SOURCE DESCRIPTION

The Orion-Monoceros complex, of which OMC-1, or Orion-KL, is but a small part, lies only 500 pc from the Sun (Genzel *et al.* 1981). Because of its proximity, it has become the prototypical region of massive star formation. The brightest infrared region of the molecular cloud complex, detected by Kleinmann and Low (1967), lies $\sim 1'$ NW of the well-known Trapezium cluster and contains extremely young and massive embedded stars which are not yet optically visible because of the cocoons of gas and dust which surround them. The Becklin-Neugebauer object (BN) (Becklin and Neugebauer 1967) is the brightest source at 2 μm, but observations at longer IR wavelengths reveal the presence of the numerous other sources. Studies of the color temperatures and dust opacities of these sources (Wynn-Williams *et al.* 1984), and of the 3.8 μm polarization vectors (Werner, Dinerstein, and Capps 1983), have shown that only BN, IRc 2, and IRc 9 are self-luminous. Of these, IRc 2 is intrinsically the brightest, providing most of the luminosity ($L = 10^5\ L_\odot$) in this region. BN appears brighter at 2 μm only because IRc 2 is buried behind a large column of obscuring material along our line of sight. The remaining infrared sources appear to be manifestations of the complex spatial structure of the surrounding molecular cloud. Other indications of the pivotal nature of IRc 2 to the structure of OMC-1 are provided by the many molecular line observations of this source.

1987ApJ...315..621B

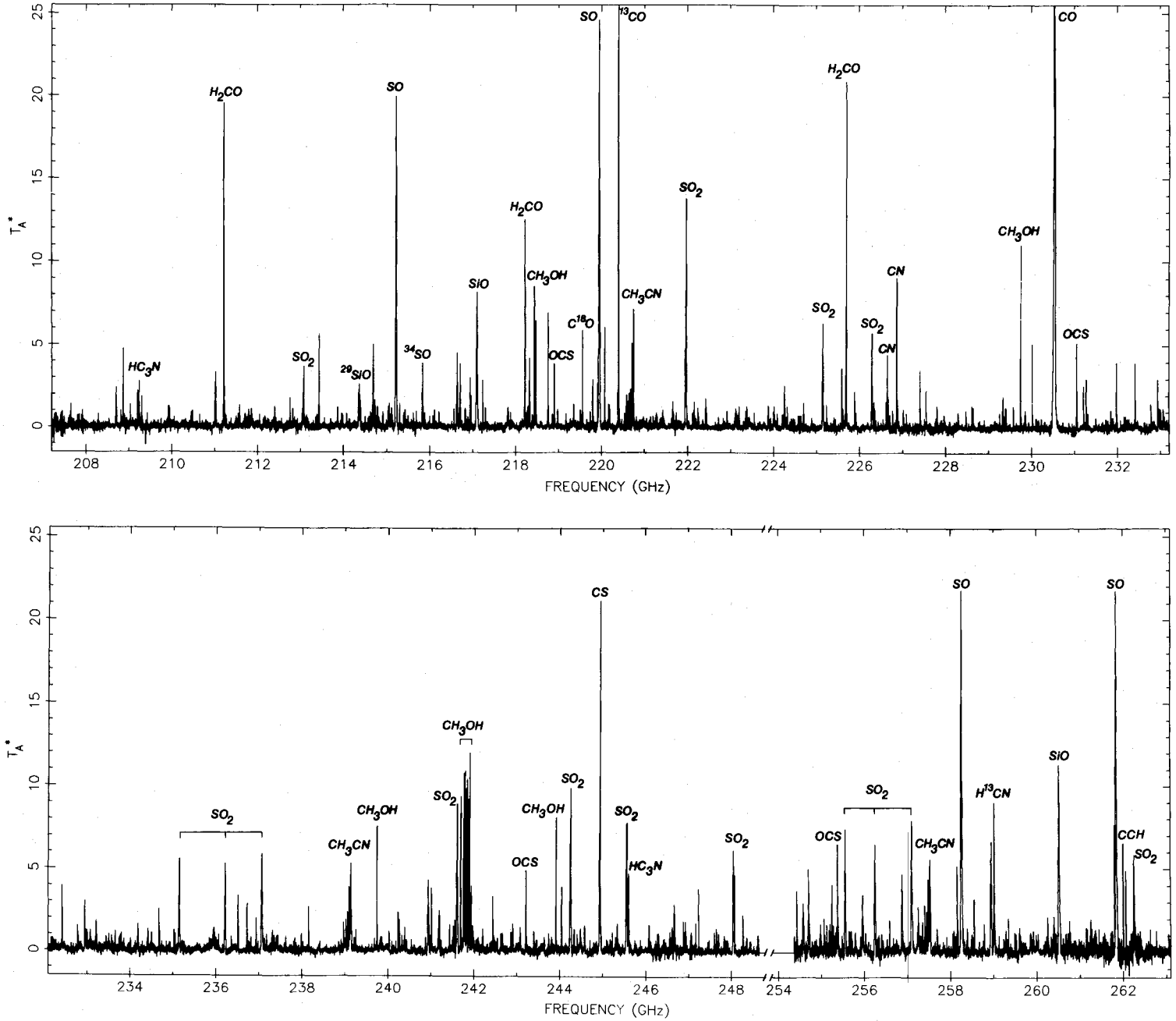

FIG. 1.—Compressed view of the OVRO spectral line survey of OMC-1

In addition to the relatively cool and quiescent gas of the Orion-Monoceros complex visible in observations of OMC-1 as a strip or "ridge" of material running SW (8 km s^{-1}) to NE (10 km s^{-1}), there are also other more turbulent components of the gas which are physically associated with IRc 2 and are attributed to outflow from that source. First discovered in Orion as high-velocity wings on H_2S and CO lines ($\Delta v_{CO} \gtrsim$ 100 km s^{-1}; Wilson, Jefferts, and Penzias 1970; Thaddeus *et al.* 1972; Zuckerman, Kuiper, and Rodriguez-Kuiper 1976), such molecular outflows now appear to be a common evolutionary phase of young stars, but little is known about the engine that drives the mass loss. The ridge or "spike" clouds are perhaps most easily visible in CS (Hasegawa 1986) or in the H_2CO $J_{K_p K_0} = 2_{12} \rightarrow 2_{11}$ transition as shown by Bastien *et al.* (1981), and lie on either side of the infrared sources. The sharp velocity gradient across the ridge has been interpreted as rotation of the overall molecular cloud structure about Orion-KL with a period of $\sim 5 \times 10^5$ yr (Lizst *et al.* 1974; Kutner *et al.* 1977; Hasegawa *et al.* 1984; Vogel *et al.* 1985). Another more spatially compact narrow-line source, labeled "the condensed ridge" by Johansson *et al.* (1984), is visible in single-dish observations of complex species such as CH_3OH or $HCOOCH_3$ and in interferometric maps of CS emission (Mundy *et al.* 1986) on the inner edge of the SW (8 km s^{-1}) cloud. Intense H_2O maser emission, located on the inner periphery of the quiescent clouds, has also been detected. Measurements of the proper motions of the H_2O masers with the VLA (Genzel *et al.* 1981) demonstrate unambiguously that the turbulent gas in Orion-KL is indeed contained in an outflow, and that this outflow or "plateau" source is highly anisotropic in nature. In addition to the high-velocity ($|\Delta v| \gtrsim 30$ km s^{-1}) plateau emission seen in CO, H_2O, and a number of other species, there also appears to be a lower velocity (18 km s^{-1}) outflow. The low-velocity emission is centered on IRc 2, as both the low-velocity H_2O maser centroids and the Hat Creek interferometric SO map show (Plambeck *et al.* 1982). The high-velocity ($|\Delta v| \gtrsim 30$ km s^{-1}) plateau is bipolar, oriented roughly orthogonal to the low-velocity SO "disk," and centered somewhat north of IRc 2, as is demonstrated by the SiO emission mapped by Wright *et al.* (1983). Immediately outside this SiO bipolar outflow is an extensive region of very hot ($T \approx 2000$ K) shock-excited H_2 vibrational emission that is adjacent to a somewhat cooler ($T \approx 750$ K) region of material first detected via high-J (up to $J = 34 \rightarrow 33$) CO emission (Gautier *et al.* 1976; Watson *et al.* 1980). Finally, lying along our line of sight toward and quite close to IRc 2 are clumps of very dense, warm material known as the "hot core," first detected in the inversion lines of NH_3 (Morris, Palmer, and Zuckerman 1980; Genzel *et al.* 1982) and recently mapped via its 2.6 mm continuum emission by Masson *et al.* (1985) and Wright and Vogel (1985).

Most of the models constructed to explain the wide variety of emission features in Orion have centered on mass outflow from IRc 2 which accelerates and alters the composition of the surrounding gas. Anisotropies in the density structure of the originally collapsing gas which produced IRc 2 are thought to be responsible for the observed anisotropy of the outflow. The higher density in the NE-SW direction outlined by the H_2CO emission slows down the flow in this direction and creates the low-velocity plateau source, while the lower density and/or faster density gradient orthogonal to this axis has allowed the flow to expand more rapidly. The low-velocity H_2O masers arise where the outflow strikes the ambient molecular cloud material. Similarly, vibrationally excited H_2 emission and the high-J CO features occur where the high-velocity wind has driven shocks into the quiescent cloud. H_2 probes a thin shell of the hottest material within the shock, while the CO emission emanates from the cooler postshock regions. Material left over from the collapse of IRc 2 is identified as the hot core, which, because of its density and mass, has not yet been dispersed by the outflow. A more complete description of the Orion-KL sources and the restrictions deduced from the line survey results on the physical models of Orion are discussed below.

III. LINE SURVEY STATISTICS AND DATA ANALYSIS

Data reduction procedures and a condensed discussion of the Caltech line survey results have been presented for the 215–247 GHz interval by Sutton *et al.* (1985) and for the 247–263 GHz region by Blake *et al.* (1986). The portion of the spectrum between 208 and 215 GHz shown in Figure 1 is not as well calibrated as the other regions and was not included in the previous publications. Only the interval from 215 to 263 GHz has actually been used in the abundance determinations that follow. A total of 29 species and 16 isotopic variants, ranging in complexity from diatomic CO and CS to the nine-atom species CH_3OCH_3 and C_2H_5CN, have been detected. Some are quite familiar and stable, but others, like CN, CCH, and HCO^+, are very reactive and most difficult to study in the laboratory.

The average noise level in the Caltech scan is $\sim$0.2–0.3 K per resolution element which, as Figure 1 indicates, places the spectral line survey near the confusion limit. Some 787 resolvable emission features have been detected in the 215–263 GHz interval, while the total line search contains over 825 lines. In comparison, the lower frequency survey of Johansson *et al.* (1984) performed at the Onsala Space Observatory reports the detection of 170 and 45 lines from Orion and IRC +10216 between 73 and 91 GHz, while the Bell Laboratories 70–145 GHz survey of Sgr B2 lists some 457 spectral features (Cummins, Linke, and Thaddeus 1986). The Onsala survey of Orion was conducted with a beam size similar to that of the Caltech survey, but the line density is roughly a factor of 2 lower. The increased density and strength of the rotational line emission in the Caltech survey as compared with the lower frequency work is due primarily to the higher intrinsic line strengths of rotational transitions at shorter millimeter wavelengths and the small telescope beam size with which the Caltech survey was conducted, making it particularly sensitive to emission from the warm, compact core of Orion-KL. By combining an extensive set of laboratory measurements with existing spectral line catalogs, over 96% of the emission lines have been identified and assigned to known interstellar species. Indeed, only 33 unidentified lines remain in the entire data set. With the exception of C_3H_2 (Thaddeus, Vrtilek, and Gottlieb 1985) and possibly PN, no "new" molecules have been identified in the 1.3 mm spectral band. Upper limits for a number of potential species, including several molecules like CO^+ and CH_3NH_2 that were previously claimed to have been identified in OMC-1, are presented along with the measured molecular abundances.

The various subsources in OMC-1 are observed simultaneously by the 30″ beam of the Caltech survey. Thus, in the absence of mapping information each of the emission components must be identified by its line profile alone. As one might expect, emission from the individual molecules in Orion is not restricted to a single region, but may arise from a complicated blend of several or all of the subsources. Figure 2 pre-

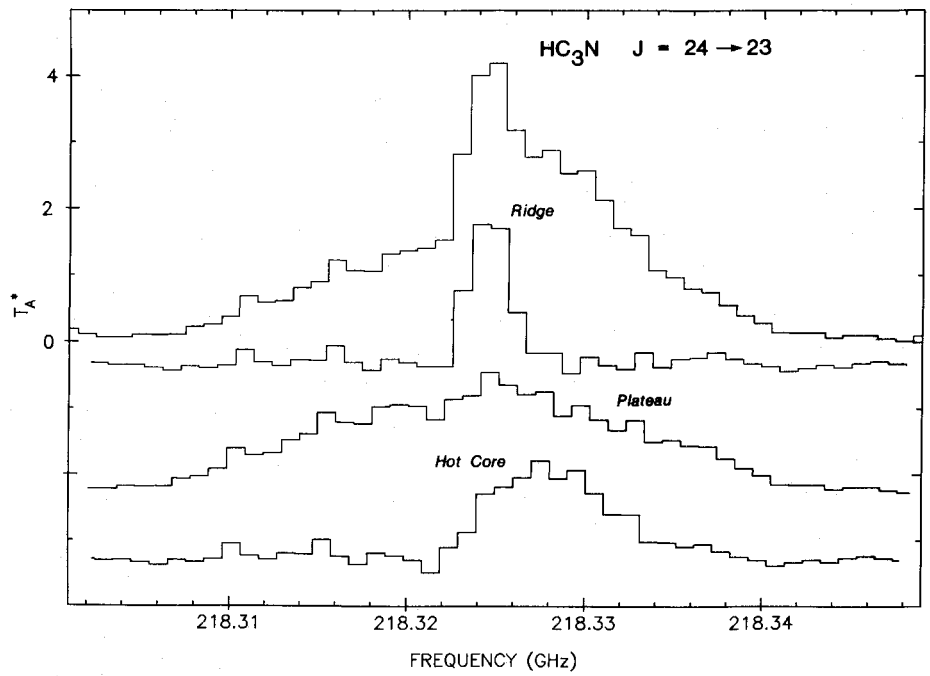

FIG. 2.—The $J = 24 \rightarrow 23$ transition of HC_3N and the Gaussian best estimates of the different kinematic components which produce its complex line profile

sents a good example of the often complex nature of the emission from Orion, the $J = 24 \rightarrow 23$ transition of HC_3N, in which all three of the distinct kinematic components are visible. As demonstrated by Figure 2, in addition to possessing different line widths, each source in Orion also appears at a characteristic radial velocity, or v_{LSR}. Any attempt at an estimate of the chemical composition of the differing regions must therefore include a deconvolution of the overall emission into its constituent parts and is subject to several sources of uncertainty which are summarized below (after Irvine *et al.* 1985).

The initial errors encountered in any astronomical study are those arising from the calibration of raw spectral data to produce the corrected antenna temperatures T_A^* and the conversion of these values into line brightness temperatures T_b via estimates of the source size. All values reported here are left as beam-averaged quantities; no corrections have been made for emission thought to arise from compact sources. The brightness temperatures of lines from the hot core and plateau regions will therefore be systematically underestimated. When several emission features are present, nonlinear least-squares fits of unconstrained Gaussian components to the emission profile such as those shown in Figure 2 have been used to separate their relative contributions. Molecules whose emission is confined to one particular source such as CH_3CCH and C_2H_5CN were analyzed first to parameterize the emission from the various kinematic components and to construct the initial guesses used in the Gaussian fits. In addition, constrained fits, which fixed the velocities and line widths of the Gaussian components at values derived from the single-component emission, were also performed on a number of test species, and no statistically significant differences were found between the excitation temperatures and column densities derived from the unconstrained and constrained fits. Although potentially biased by the initial guesses utilized, the resulting strengths and velocities were quite consistent and should be good to within the calibration errors quoted in Sutton *et al.* (1985).

Once the individual values of T_A^* have been established, it is then necessary to convert them into column densities, which requires information about the line optical depths and excitation conditions. It is impossible to estimate the line excitation and optical depth from the observation of a single line, but when many transitions of an individual molecule can be observed it is possible to estimate any deviations from thermal excitation along with the transition optical depths, particularly if the lines are not strongly saturated. For example, if we assume that the lines are optically thin and that the excitation temperature between the upper and lower levels is such that $T_{ex} \gg T_{BG}$, then the integration of the standard radiative transfer equations shows that

$$\frac{N_k}{g_k} = \frac{3kc \int T_b \, dv}{8\pi^3 \mu^2 \nu^2 S}, \tag{1}$$

where T_{BG} is the temperature of any background source (i.e. 2.7 K), ν the transition frequency, μ the permanent dipole moment, S the intrinsic line strength, and N_k and g_k are the column density and degeneracy of the upper transition state. Further assumptions must next be made about the general population distribution if total column densities are to be obtained from the observations of a single transition. If we assume that the population distribution is thermalized at a single rotational temperature T_{rot}, then N_k/g_k may be replaced by

$$\frac{N_k}{g_k} = \frac{N_T}{Q(T_{rot})} e^{-E_u/kT_{rot}},$$

where N_T is the total molecular column density summed over all the levels, E_u is the energy of the upper transition state, and $Q(T_{rot})$ is the rotational partition function at temperature T_{rot}.

The natural log of eqn (1) is therefore

$$\ln\left(\frac{3kc\int T_b\,dv}{8\pi^3\mu^2\nu^2 S}\right) = \ln\frac{N_T}{Q(T_{\rm rot})} - \frac{E_u}{kT_{\rm rot}}, \qquad (2)$$

and a plot of the log of the integrated line strength versus energy should produce a straight line whose intercept is proportional to the log of the total molecular column density and whose slope gives $T_{\rm rot}$, provided the assumptions listed above are met. Such "rotation diagrams" have been utilized in a number of previous studies (Linke, Frerking, and Thaddeus 1978; Johansson *et al.* 1984; Cummins, Linke, and Thaddeus 1986), and will be extensively applied here. Figure 3 presents rotation diagrams of those molecules in the Caltech survey for which sufficient data are available to apply this technique.

Wherever possible we have analyzed many transitions, whose optical depths were checked by observations of isotopically substituted species, to bypass the use of single transitions in the determination of molecular column densities and to increase the statistical redundancy. Errors in the derived column density stem mainly from uncertainties in the estimated source sizes which do not enter into the determination of excitation temperatures since they depend only on the *relative* transition strengths and because the spectral line survey has been uniformly calibrated. The formal errors associated with the LTE procedure were typically on the order of 15%–20%, but as Figure 3*h* illustrates, the population distributions of molecules in Orion can also be far from equilibrium. Most often these deviations arise from the large density and temperature gradients present in active molecular cloud cores, but subthermal excitation, opacity effects, radiative pumping, and other non–LTE mechanisms may also render this single-temperature approach inadequate.

It is imperative that consistent definitions of the intrinsic line strength and molecular partition function be used in equation (2) for the derived total column densities to be meaningful. In simple diatomic species and small asymmetric rotors this is quite straightforward, but for species like CH_3CN or CH_3OH in which nuclear spin statistics or internal rotation complicate matters, various definitions abound and are not interchangeable. For completeness and as an aid to future work, we present in the Appendix a brief review of the partition function definitions and dipole moments used here. Whenever possible, we have used accurate sums over individual rotational states rather than integral approximations to the partition functions (see Townes and Schawlow 1955). The extensive compilation of Poynter and Pickett (1984) has proven most useful in this regard, although there is a potential for confusion since hyperfine structure is included for some species but not for others.

In some cases (e.g., HCO^+, HCN, etc.), only one or two lines of a given molecule were detectable for which the parent isotopic transitions were most likely optically thick. For such species, isotopically substituted lines whose optical depths are small, as judged by comparing their intensities with those of the lower J transitions detected at Onsala (Johansson *et al.* 1984), have been used in conjunction with the rotational temperatures derived from molecules found to have similar excitation requirements and velocity profiles to estimate the total column densities. Chemically related species are used for the rotational temperature estimates to reduce effects of clumping or other excitation gradients which may selectively excite various species relative to each other. A number of other

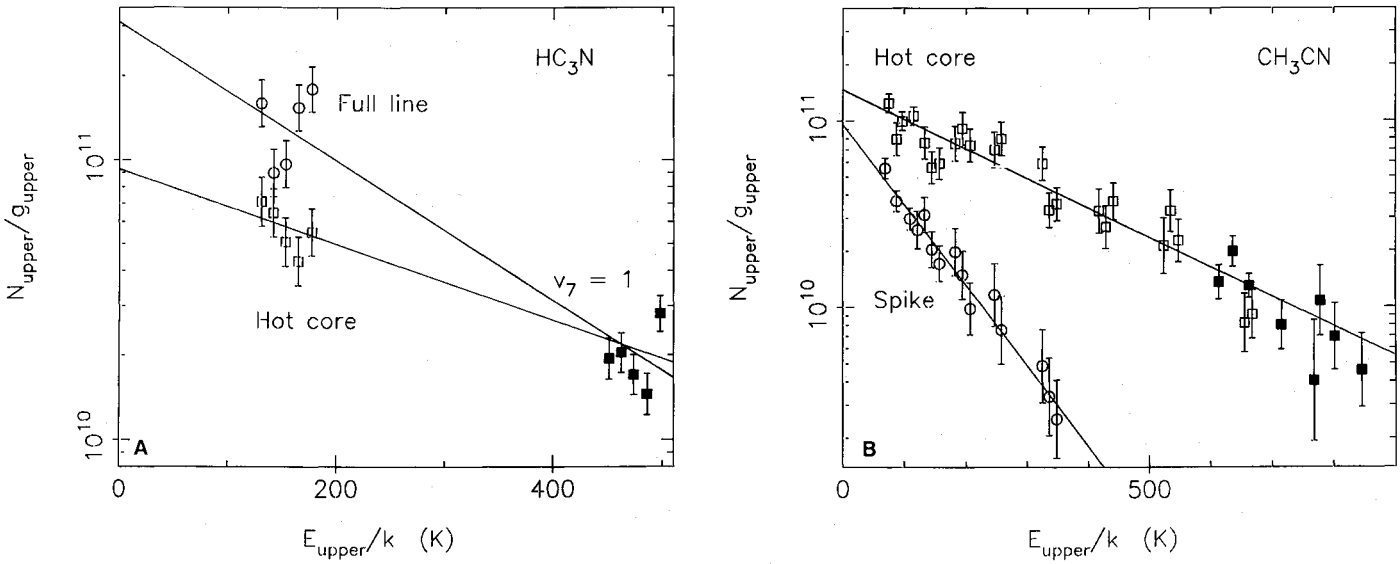

FIG. 3.—(*a*) LTE rotation diagram of HC_3N. Ground-state hot core estimates are from Gaussian fits to the line profiles, while the $v_7 = 1$ lines (filled squares) arise solely from the hot core. (*b*) LTE rotation diagrams of the spike and hot core components of the CH_3CN overall emission. Filled squares in the hot core data arise from the $v_8 = 1$ vibrationally excited bending state. (*c*) LTE rotation diagram of CH_3CCH. (*d*) LTE rotation diagrams of $^{12}CH_3OH$ and $^{13}CH_3OH$. Emission from the first torsionally excited state in CH_3OH is labeled by the filled squares. Derived column densities imply a $^{12}C/^{13}C$ ratio of 30–40. (*e*) LTE rotation diagrams of H_2CO and HDCO. Full line profiles have been used to plot the H_2CO data; no Gaussian decompositions were attempted. Note the saturation of the strong H_2CO line at 33 K. (*f*) LTE rotation diagram of H_2CS. (*g*) LTE rotation diagram of H_2CCO. (*h*) LTE rotation diagram of HNCO. Rapid spontaneous decay from the high K (higher energy) states induces the large observed populations in the low K (lower energy) levels. (*i*) LTE rotation diagram of HDO. (*j*) LTE rotation diagrams of $^{32}SO_2$ and $^{34}SO_2$. Diagram shows little evidence of saturation in the $^{32}SO_2$ lines, and is consistent with a $^{32}S/^{34}S$ ratio of 16. Filled squares arise from the $^{32}SO_2$ $v_2 = 1$ vibrationally exicited state. (*k*) LTE rotation diagram of $HCOOCH_3$. Because of the large number of lines observed, data have been averaged, or "binned," into several discrete 10 K intervals for convenience. No statistically significant differences are observed between the full data and "binned" fits. (*l*) LTE rotation diagram of CH_3OCH_3. (*m*) LTE rotation diagram of C_2H_3CN, with the data binned into 5 K intervals. (*n*) LTE rotation diagram of C_2H_5CN, with data binned into 10 K intervals where necessary.

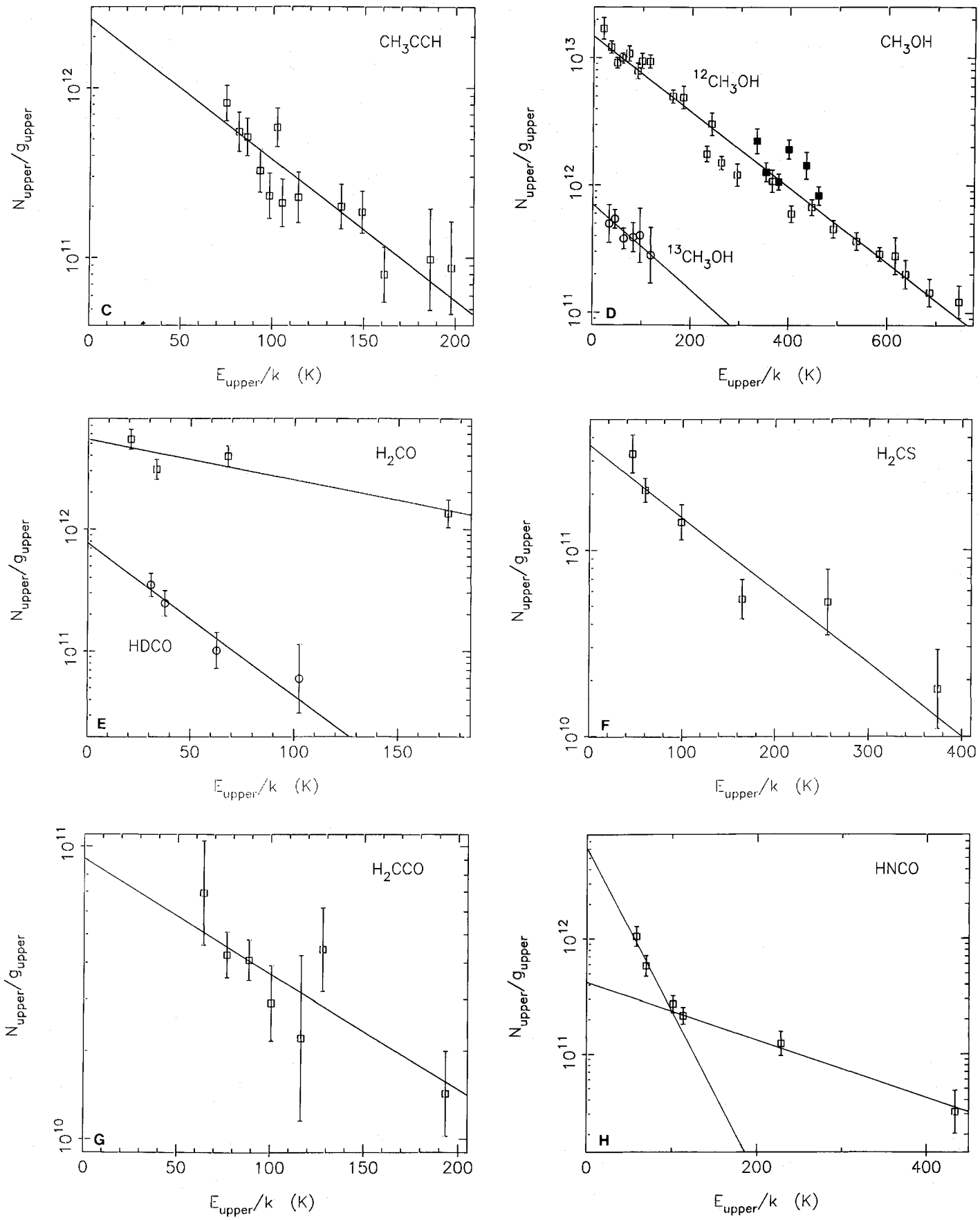

FIG. 3.—*Continued*

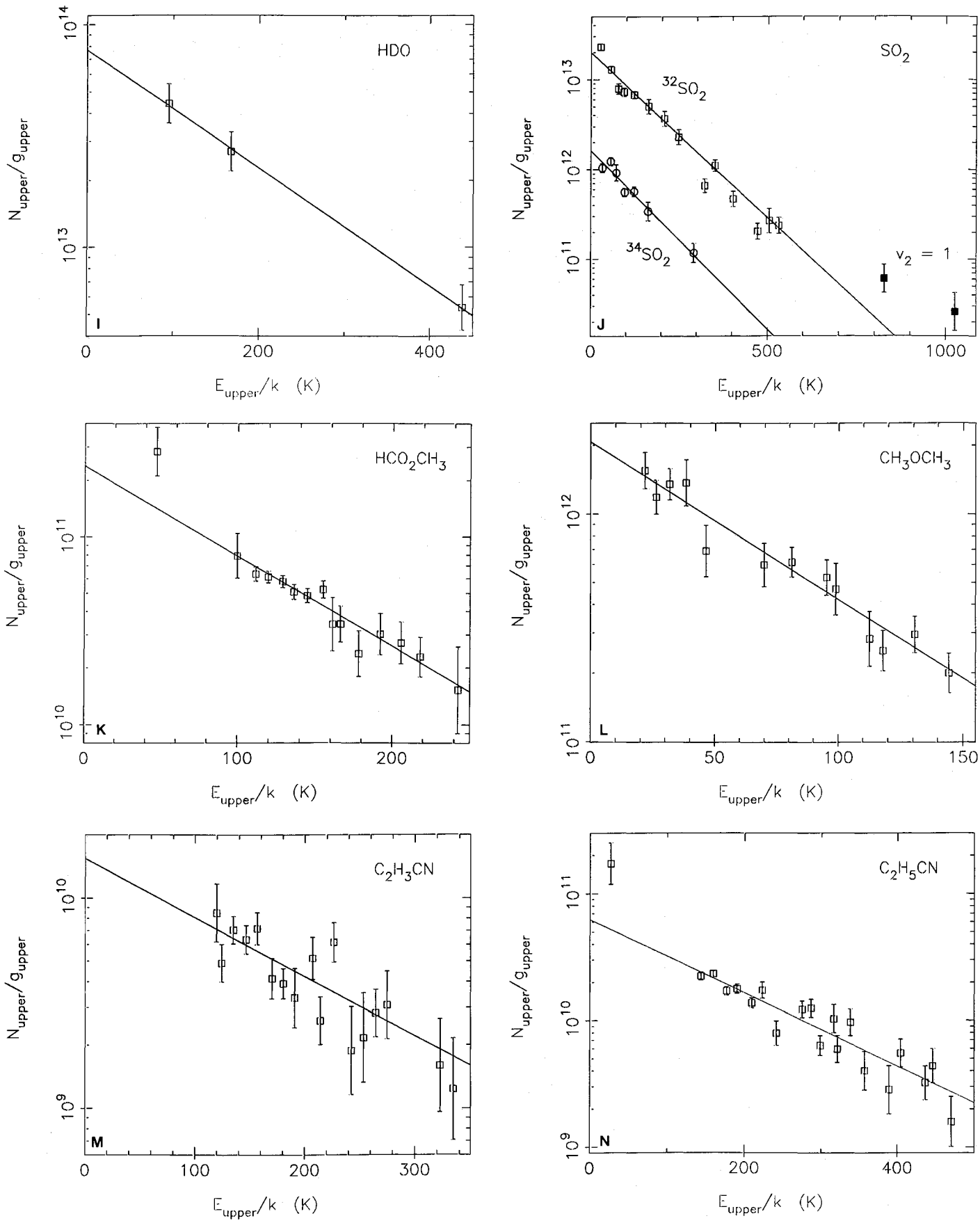

FIG. 3.—*Continued*

species, such as CN, CO^+, CCH, PN, HCOOH, etc., have also been detected or searched for, but have too few lines or lines which are too weak to be examined with the rotation diagram technique, and are therefore not likely to be optically thick. Rotational temperatures for such species have, again, been estimated using chemically related molecules with similar velocity profiles. Partition functions for these molecules have also been calculated explicitly with summations over the discrete rotational states.

Finally, the large line widths associated with the plateau emission allow the results derived from the Gaussian fits noted above to be verified for this source using a different method, first applied by Kuiper, Zuckerman, and Rodriguez-Kuiper (1981). At velocities greater than $\sim$20–25 km s^{-1} from the line center, emission from the ridge and hot core components is negligible, and emission at these velocities may safely be used to estimate molecular abundances in the plateau region. By dividing the lines of various species into the plateau emission from ^{13}CO the relative abundances of CO to the species under study were calculated assuming thermal population distributions characterized by the excitation temperature derived from an extensive LTE analysis of SO_2. ^{13}CO is utilized in place of ^{12}CO to insure that the CO emission is optically thin. The ^{13}CO abundance derived by Masson *et al.* (1984) is then used to construct column densities, which agree with those determined from the Gaussian fits to better than a factor of 2.

IV. RESULTS

By separating the various emission components seen in the Caltech survey and comparing them to previous single-dish studies, especially that of Johansson *et al.* (1984), and with interferometric maps of several key species it has been possible to construct a detailed description of the physical and chemical conditions of the emission regions in Orion. The Gaussian fits characterize the emission properties of the various subsources, while the rotation diagrams give estimates of the molecular abundances and, to some extent, the physical temperature and density of the emission regions. Rotational temperatures for easily thermalized species such as CH_3CCH should accurately reflect the kinetic temperature, while deviations from LTE can produce *rough* estimates of the H_2 density. Statistical equilibrium calculations certainly produce more accurate temperature and density estimates but at the expense of considerable complexity. A set of such calculations for the CH_3CN symmetric top has been given by Sutton *et al.* (1986). In Table 1 we present a comprehensive listing of the LTE beam-averaged column densities, excitation temperatures, and velocity characteristics of the 29 species detected in this work, and discuss below the physical properties of the OMC-1 subsources as constrained by the millimeter-wave data.

a) Physical Properties of the Orion-KL Kinematic Components

i) *Ridge Emission*

Emission from the quiescent clouds near Orion-KL appears to be composed of both an extended and a more compact component, although the distinction between these regions is often ill defined. The extended ridge emission is characterized by a velocity of $v_{LSR} \approx 9$ km s^{-1} and line widths of $\Delta v \approx 3$–4 km s^{-1} at the center of OMC-1, but elsewhere in OMC-1 the emission exhibits a shift from 8 km s^{-1} in the SW to 10 km s^{-1} in the NE (Bastien *et al.* 1981). Extended ridge emission is seen here in CO, CN, CS, SO, C_2H, C_3H_2, HCO^+, HCS^+, HNC, HCN, HC_3N, and CH_3CCH, as summarized in Table 2. The rotational temperature of the moderate dipole moment CH_3CCH symmetric top (0.75 debye), which should have a thermalized or nearly thermalized population distribution, is about $T_{rot} = 52 \pm 8$ K. Further support for a thermal, or kinetic, interpretation of the CH_3CCH rotational temperature comes from the optically thick ^{12}CO brightness temperature of 60 K for the ridge component. The kinetic temperature of the extended ridge clouds near OMC-1 would therefore appear to be $\sim$50–60 K. However, a comparison of the Caltech emission strengths of high dipole moment species such as CS, HCO^+, or HCN with those of Johansson *et al.* (1984) demonstrates that the excitation temperatures for these molecules are substantially subthermal, on the order of 15–20 K. Examination of the critical densities required to reach thermal equilibrium for the numerous molecules detected suggests that the density must be $\sim 10^5$ cm^{-3}, or slightly less. Emission away from the center of Orion-KL is strongly subthermal relative to CO for all detected species, and the density here must be $\lesssim 10^4$ cm^{-3}. Dust continuum measurements at 1 mm by Westbrook *et al.* (1976) and Elias *et al.* (1978) have been used to establish the ridge H_2 column density of $\sim 3 \times 10^{23}$ cm^{-2}.

Spatially confined ridge emission is, for the most part, still rather narrow ($\Delta v \approx 3$–5 km s^{-1}) but lies at slightly lower radial velocities of $v_{LSR} \approx 7$–8 km s^{-1}. As its name implies, this source is fairly compact and it is also characterized by the high abundances of the large oxygen-rich molecules which are found there, namely HDO, OCS, H_2CO, H_2CCO, HCOOH, CH_3OH, $HCOOCH_3$, and CH_3OCH_3 (Table 2). The small nature of this source is illustrated by a comparison of the beam-averaged OVRO T_A^* values for the $J = 5 \rightarrow 4$ band of CH_3OH with those of Boland *et al.* (1983) taken with the 3.8 m UKIRT telescope. Boland *et al.* report a maximum brightness temperature of 4.0 K in the $J_K = 5_{\pm 4} \rightarrow 4_{\pm 4}$ components for which we report an antenna temperature of 11.8 K, implying a source size of $\lesssim 30''$. A source of this size is also inferred from interferometric studies of the 25 GHz CH_3OH masers (Matsakis *et al.* 1980) and of the 6 cm H_2CO emission mapped at the VLA by Johnston *et al.* (1983), which are also coincident with the HDO and CH_3OCH_3 emission mapped by Olofsson (1984). These maps show that the spatially compact ridge is located on the edge of the SW 8 km s^{-1} cloud near IRc 5.

The spatially confined ridge source also appears to be a good deal warmer than the spatially extended material. For example, rotation diagrams of H_2CS, H_2CCO, CH_3OH, and $HCOOCH_3$ among others yield values of T_{rot} between 90–140 K. Since it is observed in so many states, emission from CH_3OH serves as the best cloud temperature "thermometer," and although its v_{LSR} is roughly constant, there is also a clear line width and temperature gradient as a function of excitation energy. The lowest energy lines are characterized by line widths of 3.3 km s^{-1} and a rotational temperature of 120–140 K, while the highest energy lines, including those from the first torsionally excited state, have line widths of $\sim$6.5–9.5 km s^{-1} and a rotational temperature in excess of 200 K. Spontaneous emission rates of the torsionally excited lines require central densities of $\gtrsim 10^7$ cm^{-3} for purely collisional population of the upper transition states, which may therefore also be populated radiatively. The geometrical location, radial velocity, temperature gradient, and chemical composition of the compact ridge source is suggestive of a linkage between it and the plateau source, in which outflow from IRc 2 interacts with the 8 km s^{-1} cloud thereby compressing, heating, and

TABLE 1

MOLECULAR COLUMN DENSITIES AND GAUSSIAN DECOMPOSITIONS FOR THE EMISSION FROM OMC-1

Species	T_{rot}[a] (K)	N (mol cm^{-2})	v_{LSR} (km s^{-1})	Δv (km s^{-1})	Notes
Ridge: $N_{H_2} = 3 \times 10^{23}$ cm^{-2} [b]					
Extended:					
C I	(20)	$\gtrsim 7.5 \times 10^{17}$	9.5	5.0	1
CO	60	1.5×10^{19}	8.7	4.3	2, 3
CN	(60)	1.0×10^{15}	8.8	4.4	4
NO	(60)	$\lesssim 1.5 \times 10^{16}$	~9.0	~4.0	4
C_2H	(60)	1.6×10^{15}	8.8	~4.0	4
CH_3CCH	52 ± 8	1.0×10^{15}	9.3	3.8	5
NH_3	(60)	1.5×10^{17}	9.0	7.0	4, 6
CS	(20)	7.5×10^{14}	8.9	4.4	7
HCO^+	(20)	7.0×10^{14}	8.7	3.6	7, 8
HCS^+	(60)	1.6×10^{13}	~9.0	~4.0	4
HCN	(20)	1.5×10^{15}	9.0	3.5	7, 8
DCN	(20)	5.1×10^{12}	...	...	7, 8
HNC	(20)	1.6×10^{14}	8.3	3.3	7, 8
DNC	(20)	2.3×10^{12}	...	...	7, 8
HC_3N	(60)	4.0×10^{13}	8.9	3.3	4
C_3H_2	(20)	2.6×10^{13}	~9.0	~7.0	9
HNCO	35 ± 3	$\lesssim 6.5 \times 10^{14}$	8.4	~4.3	5, 10
HDCO	32 ± 7	5.6×10^{13}	8.8	~4.0	5
SiO	(20)	$< 1.0 \times 10^{14}$	...	...	11
SO	(20)	$\lesssim 2.8 \times 10^{14}$	8.4	3.4	8, 11, 12
SO_2	(60)	$< 1.0 \times 10^{15}$	7.7	4.2	4, 11, 12
HCO	(60)	$< 1.0 \times 10^{13}$	...	...	4, 11
C_3N	(20)	$< 5.0 \times 10^{12}$	...	...	11
C_4H	(20)	$< 2.5 \times 10^{12}$	...	...	11
HC_5N	(20)	$\lesssim 7.0 \times 10^{12}$	...	...	13
Compact:					
PN	(90)	$\lesssim 3.0 \times 10^{12}$	8.0	3.8	4, 14
PO	(90)	$< 5.0 \times 10^{13}$	...	...	4
OCS	(75)	1.0×10^{15}	7.8	3.7	15
HDO	(90)	1.9×10^{14}	7.0	2.0	4
CH_3CN	101 ± 9	9.6×10^{13}	8.4	4.0	5
CH_3OH	146 ± 3	3.5×10^{16}	8.1 7.2	3.3 9.6	5, 16
H_2CO	(90)	5.0×10^{15}	8.6	3.8	8
H_2CS	116 ± 17	4.8×10^{14}	7.6	4.1	5
H_2CCO	110 ± 36	2.0×10^{14}	8.2	4.0	5
CH_3OCH_3	63 ± 5	3.0×10^{15}	7.9	3.6	5
$HCOOCH_3$	90 ± 10	2.6×10^{15}	7.9	3.9	5
HCOOH	(90)	1.5×10^{14}	8.0	3.9	4
CH_3CHO	(90)	$\lesssim 5.0 \times 10^{13}$	8.3	3.9	4
CH_3NH_2	(90)	$< 3.0 \times 10^{14}$	...	...	4, 11
C_2H_5OH	(90)	$< 1.5 \times 10^{14}$	...	...	4, 11
NH_2CHO	(90)	$< 3.0 \times 10^{13}$	...	...	4, 11
NH_2CN	(90)	$< 3.0 \times 10^{13}$	...	...	4, 11
Plateau: $N_{H_2} \lesssim 5 \times 10^{22}$ cm^{-2} [c]					
CO	(100)	6.5×10^{18}	7.7	49.6	2, 14
CS	(100)	1.2×10^{15}	7.1	23.2	4
OCS	(100)	2.8×10^{15}	5.3	19.0	4, 17
SiO	(100)	1.5×10^{15}	7.0	34.0	4
SO	(100)	2.8×10^{16}	7.8	28.0	4
SO_2	106 ± 3	2.8×10^{16}	7.7	25.2	5, 14
HCN	(100)	1.5×10^{16}	8.6	27.0	4, 8
HC_3N	(100)	1.8×10^{14}	7.7	28.5	4
H_2S	(100)	5.0×10^{15}	7.2	22.7	4
HDO	(100)	9.0×10^{14}	...	...	4
H_2CO	(100)	1.7×10^{15}	8.9	42.2	4
Hot Core: $N_{H_2} \approx 1 \times 10^{23}$ cm^{-2} [c]					
CO	(200)	1.0×10^{19}	6.2	10.5	2, 14, 18
SO	(200)	$\lesssim 1.7 \times 10^{15}$	6.7	10.9	4, 12
SO_2	(200)	$\lesssim 2.0 \times 10^{15}$	2.6	6.9	4, 12
HDO	164 ± 23	4.4×10^{15}	5.7	9.1	5
H_2CO	166 ± 70	2.2×10^{15}	6.9	12.7	5
HNCO	182 ± 45	4.8×10^{14}	6.6	9.1	5
HCN	(200)	2.5×10^{16}	5.8	12.6	4, 8
DCN	(200)	5.9×10^{13}	6.0	11.7	4, 8
HC_3N	312 ± 35	1.3×10^{14}	3.8	10.0	5
CH_3CN	274 ± 12	6.5×10^{14}	5.0	10.3	5
C_2H_3CN	154 ± 28	1.5×10^{14}	5.0	8.6	5
C_2H_5CN	150 ± 9	8.2×10^{14}	5.0	11.4	5

TABLE 2

SUMMARY OF OMC-1 EMISSION COMPONENT PARAMETERS

Source	v_{LSR} (km s^{-1})	Δv (km s^{-1})	T_{rot} (K)	n (cm^{-3})	θ_{source}	N_{H_2} (cm^{-2})	Molecules Detected
Extended ridge	9	4	55–60	$\sim 10^5$	Extended	3×10^{23}	CN, CO, CS, NO, SO, CCH, C_3H_2, CH_3CCH, HCO^+, HCS^+, HCN, HNC, HC_3N
Compact ridge	7–8	3–5	80–140	$\gtrsim 10^6$	$\lesssim 30''$	...	PN(?), OCS, HDO, H_2CO, H_2CS, HCOOH, CH_3CHO(?), CH_3CN, H_2CCO, CH_3OH, $HCOOCH_3$, CH_3OCH_3
Plateau	7–8	$\gtrsim$20–25	95–150	$\gtrsim 10^6$	$\lesssim 20''$	$\lesssim 1 \times 10^{23}$	CO, CS, SiO, SO, SO_2, OCS, H_2S, HDO, H_2CO, HCN, HC_3N
Hot core	3–5	5–10	150–300	$\gtrsim 10^7$	$\lesssim 10''$	1×10^{24}	CO, HDO, H_2CO, HNCO, HCN, HC_3N, CH_3CN, C_2H_3CN, C_2H_5CN

altering the chemical composition of the ambient molecular cloud material (Johansson *et al.* 1984; Irvine and Hjalmarson 1984, p. 15).

ii) *Plateau Emission*

Emission from the plateau source is detected here in CO, CS, SiO, SO, SO_2, OCS, H_2S, HDO, H_2CO, HCN, and HC_3N, as Table 2 shows. It is characterized by the v_{LSR} of 7–8 km s^{-1} also found for the compact ridge source but is spatially distinct and has substantially greater line widths of at least $|\Delta v| \gtrsim$ 20–25 km s^{-1} for the high-velocity outflow, and $|\Delta v| \approx 18$ km s^{-1} for the lower velocity material. Interferometer maps of SO, SiO, and CO show that the source size is less than $\theta_{plateau} \lesssim 20''$ for both components (Plambeck *et al.* 1982; Wright *et al.* 1983; Masson *et al.* 1984). The thermalized emission from high dipole moment species such as SO_2 implies that the densities in the plateau exceed 10^6 cm^{-3}, consistent with the estimated source mass of 10–20 $M_\odot$ and the source size noted above. Higher density clumps of material are also evident through the presence of very fragile molecular species such as H_2CO. A rotation diagram analysis of SO_2 produces an excitation temperature on the order of 100 K, but, as with the compact ridge material, a range of excitation is evident. For example, the highest excitation lines of SO_2 are best fitted by a T_{rot} of at least 150–175 K. From the derived column density of SO_2 and the intensity ratios of various SO_2 transitions to the $J = 2 \rightarrow 1$ line of ^{13}CO, the plateau is estimated to have a peak H_2 column density of $\lesssim 1 \times 10^{23}$ cm^{-2} for an assumed CO fractional abundance of $f(CO/H_2) \approx 1.2 \times 10^{-4}$. This value is in good agreement with the column density given by the 2.6 mm dust continuum maps (Masson *et al.* 1985; Wright and Vogel 1985) but stands in contrast to the value of $\sim 10^{24}$ cm^{-2} inferred by Plambeck *et al.* (1982), and places important constraints on the nature of the outflow.

Whereas Plambeck *et al.* (1982) conclude that the low-velocity plateau is composed of a rather massive, organized disk or "doughnut" of gas and dust which channels the higher velocity outflow, the low column density derived above is more supportive of the "clumpy cavity" model of Wynn-Williams *et al.* (1984) in which outflowing winds from IRc 2 have only partially evacuated an irregular cavity which surrounds it. Easily destroyed molecules such as H_2CO are confined to small, dense clumps of matter embedded in the outflow, while species such as SO trace out a relatively thin shell of material on the outer boundaries of the cavity where the outflow is decelerated by the dense molecular cloud. The high-velocity plateau is interpreted as expanding more forcefully along the most rapid density gradients within the cavity.

iii) *Hot Core Emission*

As noted in the introduction, the hot core is a particularly warm, compact, and dense region of material located immediately adjacent to IRc 2. In either a cavity or a disk model the hot core is simply a very large, dense clump (or an ensemble of smaller clumps) left over from the formation of IRc 2 and not yet significantly disrupted by the outflow. The v_{LSR} and Δv (FWHM) of the hot core are not so well defined as those of the plateau or ridge sources, but lie predominantly in the 3–5 and 10–15 km s^{-1} range, respectively. Molecules detected in this source include CO, HDO, H_2CO, HNCO, HCN, HC_3N, CH_3CN, C_2H_3CN, and C_2H_5CN (see Table 2). Because of its close proximity to IRc 2, a considerable range of excitation temperatures is present in the hot core. The temperature of the gas and dust surrounding an embedded stellar source should fall off roughly as $r^{1/2}$. Thus, the species requiring highest excitation should be closest to IRc 2, and indeed, the energetic high-J ground state and vibrationally excited lines of HC_3N and CH_3CN have excitation temperatures on the order of 285–350 K, have quite small source sizes ($\theta \lesssim 3$–$5''$), and are centered on IRc 2. Lower rotational temperatures of $\sim$110–200 K and more extended source sizes are derived from the ground-

NOTES TO TABLE 1

[a] Temperatures in parentheses are assumed values.

[b] Ridge H_2 column density from dust continuum measurements.

[c] Plateau and hot core H_2 column densities are beam not source averaged.

NOTES.—(1) Taken from Phillips and Huggins 1981. (2) CO brightness temperature gives T_{kin} of source. (3) N(CO) from $C^{17}O$, $C^{18}O$ line intensities and solar isotope ratios. (4) T_{rot} assumed equal to T_{kin}. (5) Rotation diagram fit to give T_{rot} and N. (6) From the values of $\tau_p(J_K = 1_0 \rightarrow 0_0)$ estimated by Keene *et al.* 1982. (7) Subthermal T_{rot} as judged by OVRO and Onsala data. (8) Δv, v_{LSR}, and N_{col} from average of fits to isotopic lines. (9) Identified by Thaddeus, Vrtilek, and Gottlieb 1985, large Δv from line blend. (10) From a Gaussian decomposition of the lowest K_p lines. (11) Upper limits only. (12 N estimated from a Gaussian decomposition of velocity line shape. (13) Limit from Johansson *et al.* 1984. (14) Rotation diagrams of selected species gives T_{kin} of source. (15) T_{rot} from Goldsmith and Linke 1981. (16) Gaussian decomposition into a "cool" and "warm" compact ridge component. (17) v_{LSR} implies hot core also? (18) From a Gaussian decomposition of ^{13}CO and Masson *et al.* 1984.

state lines of $^{15}NH_3$, C_2H_3CN, and C_2H_5CN (Hermsen *et al.* 1985). The equalization of the ground and excited vibrational state excitation temperatures via purely collisional means would require densities in excess of 10^{10} cm^{-3}, but radiative pumping is likely to be important throughout this source and could produce excitation temperatures similar to those observed over a radius of some 5″ (Goldsmith *et al.* 1983). A statistical equilibrium analysis of the CH_3CN ground vibrational state hot core emission (Sutton *et al.* 1986) is most consistent with a kinetic temperature of at least 200 K and a minimum density of 10^6 cm^{-3}. Correcting the measured ^{13}CO antenna temperature with the source size derived by Masson *et al.* (1984) from an interferometric study of CO results in an estimated peak hot core H_2 column density of $\sim 10^{24}$ cm^{-2}, in agreement with the recent continuum maps by Masson *et al.* (1985) and Wright and Vogel (1985) and the ammonia hot core emission mapped at the VLA (Genzel *et al.* 1982).

b) *Molecular Abundance Determinations*

Nearly all of the theoretical chemical models of interstellar molecular clouds calculate the absolute fractional abundance $f(X)$ of a species X relative to the most abundant interstellar molecule, H_2, defined by $f(X) = N(X)/N(H_2)$. For a direct comparison of the observational and theoretical results it is necessary to convert the column densities $N(X)$ listed in Table 1 into absolute fractional abundances $f(X)$, which requires a number of additional assumptions. First of all, for a meaningful comparison of the abundances of various species it must be assumed that they sample similar regions of space; that is, the source or subsources should be chemically and physically uniform. Fortunately, in Orion the major subsources are clearly recognizable through their distinct spectral signatures and spatial locations, but small-scale variations in their density and size can still induce considerable error. Second, the abundance relative to hydrogen of some trace molecule, usually CO, must be known accurately since H_2 is in general unobservable in molecular clouds. Any errors in the abundance of this "standard" will be systematically transferred to all other species. CO is typically chosen because it is the most ubiquitous and abundant trace molecule and because its abundance is not expected to vary strongly with density and temperature. The CO/H_2 abundance is not easily observable directly, but is usually inferred from observations of the CO and H_2 abundances as a function of the visual extinction by dust, A_v. Provided the gas-to-dust ratio and the extinction properties of dust are known, the CO/H_2 ratio may be estimated. This procedure assumes that CO is a valid tracer of H_2; any gradients in the CO/H_2 abundance ratio are unknown. The absolute fractional abundances of other trace species X are obtained from the ratio of the column densities of X and CO, or

$$f(X) = \frac{N(X)}{N(H_2)} = \frac{N(X)}{N(CO)} \frac{N(CO)}{A_v} \frac{A_v}{N(H_2)} . \quad (3)$$

As Irvine *et al.* (1985) note, since CO is very easily excited this procedure may well underestimate molecular fractional abundances, particularly for those species whose excitation requirements are severe. The uncertainties are somewhat smaller in Orion because the gas there is relatively warm and in Orion-KL it has been possible to obtain direct estimates of the CO/H_2 ratio (see Wilson *et al.* 1986; Watson 1982; Scoville *et al.* 1983). Absolute fractional abundances have been calculated using a canonical value of $f(CO) \approx 5 \times 10^{-5}$ in the ridge sources and $f(CO) \approx 1.2 \times 10^{-4}$ in the hot core and plateau.

The column densities from Table 1 have been converted into fractional abundances, and the results are presented in Table 3. The net effect of the numerous assumptions required to obtain abundances relative to H_2 from the observations of interstellar molecular rotational emission lines are such that the individual fractional abundances are probably not accurate to better than a factor of 5–10. However, since the bulk of the data has been acquired in a uniformly calibrated spectral scan, the *relative* abundance values should be considerably more accurate. For example, consider the plateau abundances obtained from the ratios of high-velocity line emission. Provided the source sizes do not vary greatly from molecule to molecule, the beam-averaged T_A^* values for optically thin lines should be equally in error for all species, and any calibration mistakes, like the uncertainty in the CO/H_2 ratio, will be canceled out in a comparison of the relative abundances.

In summary, we see from Tables 1 and 3 that the Orion molecular cloud is not chemically homogeneous, but is instead composed of a number of sources whose chemical compositions vary considerably. Indeed, while the reactive carbon-rich species CN, C_2H, and C_3H_2 are quite abundant in the extended molecular material, they have not been detected, and are much rarer, in the other sources. The hot core and condensed ridge sources appear to share some similar physical properties, but one appears highly nitrogen-rich, while the other is dominated by heavy oxygen-containing species. Plateau emission has very strong signatures from silicon and sulfur molecular species which are not evident elsewhere, but also contains appreciable quantities of simple and moderately complex molecules such as HDO and H_2CO found in both the ridge and hot core sources. The unification of these seemingly disparate results for the various emission regions and a more thorough discussion of the effects of mass outflow on the chemical composition of molecular clouds is presented in § V.

c) *Isotopic Ratios*

As matter cycles between stars and the clouds from which they form, the isotopic composition of the interstellar gas is affected by the nuclear processing of matter in stellar interiors. Thus, a comparison of interstellar and terrestrial isotopic ratios can trace evolutionary changes in the composition of the interstellar medium, and knowledge of the isotopic ratios in molecular clouds is therefore important because they provide clues to the understanding of the interplay of matter in the Galaxy. The observations of lighter elements such as D and Li produced in the big bang can also, in principle, place important constraints on cosmological models.

Within the observational errors, the estimated ^{15}N, ^{29}Si, and ^{30}Si abundances appear to be similar to their terrestrial values, in agreement with extensive galactic surveys of HCN, HNN^+, and SiO (Wannier, Linke, and Penzias 1981; Linke, Guélin, and Langer 1983; Penzias 1981). However, the $^{18}O/^{17}O$ and $^{32}S/^{34}S$ ratios are lower than those found in the solar system by ~30%–40%. The $J = 2 \rightarrow 1$ $C^{18}O$ and $C^{17}O$ lines produce a $^{18}O/^{17}O$ isotopic ratio of 3.5 (terrestrial ratio = 5.5), while the many ^{34}SO and $^{34}SO_2$ transitions available are consistent with a $^{32}S/^{34}S$ ratio of 14–16, compared to the terrestrial value of 23. Similar results have been found for the oxygen isotopes by Penzias (1981), and for the sulfur species by Schloerb *et al.* (1983) and Johansson *et al.* (1984).

The $^{12}C/^{13}C$ and H/D ratios are lower still in a relative sense, but isotopic fractionation makes a detailed interpretation of the observed ratios rather uncertain, particularly for

TABLE 3

MOLECULAR FRACTIONAL ABUNDANCES IN THE OMC-1 SUBSOURCES

Species	$f(X)$ $[N(X)/N(H_2)]$
Extended Ridge:	
NO	$\lesssim 5.0 \times 10^{-8}$
CO	5.0×10^{-5}
CS	2.5×10^{-9}
CN	3.3×10^{-9}
HNC	5.3×10^{-10}
HCN	5.0×10^{-9}
C_2H	$\sim 5.3 \times 10^{-9}$
C_3H_2	8.7×10^{-11}
HDCO	1.9×10^{-10}
HCO^+	2.3×10^{-9}
HCS^+	5.3×10^{-11}
HC_3N	1.3×10^{-10}
DNC	7.7×10^{-12}
DCN	1.7×10^{-11}
CH_3CCH	3.3×10^{-9}
HC_5N	$\lesssim 2.3 \times 10^{-11}$
SiO	$< 3.3 \times 10^{-10}$
HCO	$< 3.3 \times 10^{-11}$
SO	$\lesssim 9.3 \times 10^{-10}$
SO_2	$\lesssim 3.3 \times 10^{-9}$
HNCO	$\lesssim 2.2 \times 10^{-9}$
C_3N	$< 1.7 \times 10^{-11}$
C_4H	$< 0.8 \times 10^{-11}$
CO^+	$< 1.0 \times 10^{-12}$
Compact Ridge:	
PN	$\lesssim 1.0 \times 10^{-11}$
PO	$< 1.7 \times 10^{-10}$
OCS	3.3×10^{-9}
HDO	6.3×10^{-10}
H_2CO	1.7×10^{-8}
H_2CS	1.6×10^{-9}
CH_3OH	1.2×10^{-7}
CH_3CN	3.2×10^{-10}
HCOOH	5.0×10^{-10}
H_2CCO	6.7×10^{-10}
CH_3OCH_3	1.0×10^{-8}
$HCOOCH_3$	8.7×10^{-9}
NH_2CH	$< 1.0 \times 10^{-10}$
CH_3NH_2	$< 1.0 \times 10^{-9}$
CH_3CHO	$\lesssim 1.7 \times 10^{-10}$
C_2H_5OH	$< 5.0 \times 10^{-10}$
CH_3COOH	$< 5.0 \times 10^{-9}$
NH_2CHO	$< 1.0 \times 10^{-10}$
Plateau:	
CO	1.2×10^{-4}
CS	2.2×10^{-8}
SO	5.2×10^{-7}
SiO	2.8×10^{-8}
OCS	5.2×10^{-8}
SO_2	5.2×10^{-7}
HCN	2.8×10^{-7}
HC_3N	3.3×10^{-8}
HDO	1.7×10^{-8}
H_2S	9.8×10^{-8}
H_2CO	3.1×10^{-8}
Hot Core:	
CO	1.2×10^{-4}
SO	$\lesssim 2.0 \times 10^{-8}$
SO_2	$\lesssim 2.4 \times 10^{-8}$
HDO	5.3×10^{-8}
H_2CO	2.6×10^{-8}
HNCO	5.8×10^{-9}
HCN	3.0×10^{-7}
DCN	7.1×10^{-10}
CH_3CN	7.8×10^{-9}
HC_3N	1.6×10^{-9}
C_2H_3CN	1.8×10^{-9}
C_2H_5CN	9.8×10^{-9}

deuterium. Isotopic fractionation is an unavoidable consequence of the ion-molecular scheme used to model low-temperature interstellar chemistry because of the rapid isotopic exchange reactions

$$^{13}C^+ + {}^{12}CO \rightarrow {}^{12}C^+ + {}^{13}CO + 35\ K\ , \quad (4)$$

$$H_3^+ + HD \rightarrow H_2D^+ + H_2 + 298\ K\ , \quad (5)$$

which can enhance or deplete the isotopic ratios in different species. The equilibria of reactions (4) and (5), and thereby the isotopic fractionation, can vary considerably at the low temperatures characterizing the interstellar medium because their small exothermicities, induced by differences in the zero-point energies of the isotopically substituted species, are well matched to the kinetic temperatures of typical molecular clouds. Fractionation is most apparent in the H/D ratio which may be raised by factors of 10,000 in the coldest clouds, as is illustrated by the high HDO and HDCO abundances observed here. Large-scale time-dependent computer models have also predicted that the $^{12}C/^{13}C$ ratio can become significantly fractionated via equation (4), with ^{13}C abundances enhanced in CO to values near $^{12}C/^{13}C \approx 20$–30 and depleted by similar amounts in molecules formed from C^+ such as HCN or CH_3OH when the cloud temperature is below 50 K. Differential photodissociation of the ^{13}CO and ^{12}CO molecules causes the $^{12}C/^{13}C$ ratio to vary as a function of depth into the cloud because like H_2, CO can "self-shield" itself against photodissociation to some extent (Glassgold, Huggins, and Langer 1985). In contrast to these theoretical expectations, all of the isotopically substituted species detected in the Caltech and Onsala surveys are consistent with a $^{12}C/^{13}C$ ratio of 40 throughout OMC-1. Numerically, it is found that $^{12}CO/^{13}CO$ is ~ 40 in the high-velocity plateau gas where optical depths are low, while HCN, HNC, OCS, H_2CO, and CH_3OH all produce values in range of 30–40 (Johansson *et al.* 1984; Blake *et al.* 1984). As Johansson *et al.* note, these low values agree with the optically determined $^{12}CO/^{13}CO$ ratio of 55 ± 11 (Wannier, Penzias, and Jenkins 1982) and may indicate an evolutionary decrease of the galactic $^{12}C/^{13}C$ content, but the uncertainties are still considerable and values nearer to the terrestrial ratio of 89 have also been derived in Orion (Scoville *et al.* 1983; Snell *et al.* 1984).

V. DISCUSSION

The remarkable chemical diversity of the differing kinematic components of OMC-1 derived in § III suggests that both the chemical and physical composition of molecular clouds may be substantially altered by the process of star formation. In order to more fully address the mechanisms responsible for the production of interstellar molecules and the potential impact of star formation on the chemistry of molecular clouds, a more detailed analysis of the observed chemistry is presented. The composition of the extended Orion component will be examined first since it should be most directly comparable to the observational results on other quiescent clouds, and since it should most closely reflect the composition of OMC-1 prior to the recent onset of star formation. We shall then address the composition of the other sources in Orion, comparing them when possible with the abundances found in other similar clouds, with the general modifications of "standard" molecular cloud chemistry resulting from star formation in the cloud core, and with the predictions of various detailed chemical models incorporating the expected physical processes (i.e., shocks) associated with massive star formation.

a) The Extended Ridge

Early models of interstellar chemistry dealt nearly exclusively with ion-molecule reactions because of their rapid rates at low temperatures and the ease with which large networks of coupled equations could be traced, and also concentrated on quiescent, isolated objects because of their simple structure and presumed homogeneity. Such models successfully predicted the abundances of many simple species, most notably those of molecular ions such as HCO^+ and HNN^+, before they were identified. Because they neglected photodissociation, surface processes on grains, shocks, etc., such models predicted modest variations in source composition with density provided the initial conditions were set to be the same. In contrast, observational work on simple interstellar species such as CO, HCN, and H_2CO (Wootten *et al.* 1978, 1980; Wootten, Snell, and Evans 1980*b*) had suggested that their abundances declined rapidly as the densities of the regions studied increased. This was interpreted primarily as the depletion of molecules onto grain mantles. For sticking coefficients on the order of unity, grain-molecule adsorption times are about $t_{\rm stick} \approx 2.5 \times 10^9/n_{\rm H_2}$ yr, where $n_{\rm H_2}$ is the cloud H_2 density per cm^3. Even for a moderate density region with $n_{\rm H_2} = 10^4$ cm^{-3} the adsorption time of $t_{\rm stick} \approx 2.5 \times 10^5$ yr is significantly shorter than the inferred cloud lifetimes ($\sim 10^7$ yr), and the density-dependent adsorption of gas-phase species onto grain mantles would therefore be expected to be a serious problem in maintaining the high observed abundances of molecular species in the dense cores of molecular clouds. Indeed, the depletion of atoms and molecules onto grain surfaces has recently been *directly* measured via 4.6 μm observations of the CO $v = 0 \rightarrow 1$ band by Hall (1984), who finds there is a marked decrease in $N(CO)/A_v$ for $T_{\rm rot}(CO) < 20$ K compared to clouds for which $T_{\rm rot} > 20$ K.

However, since the more accurately calibrated data from the spectral line surveys conducted at Onsala, Caltech, and Bell Laboratories have supplanted the earlier exploratory work in the near millimeter-wave region, it has become clear that the abundances of simple species in various clouds of quiescent gas are, in fact, rather uniform, as will be shown below. For example, Table 4 presents a listing of the abundances of a number of species in the Orion, Taurus, and Sagittarius molecular clouds derived from the Caltech, Onsala, and Bell Labs spectral line surveys, along with predictions from the extensive time-dependent chemical model of Herbst and Leung (1986). The two theoretical predictions apply to those abundances found under steady state conditions ($t > 10^7$ yr) for clouds containing a solar C/O ratio (C/O ≈ 0.4) and an enhanced C/O ratio of 1.28. Also included in Table 4 are the abundances of more complex molecules such as CH_3CN and CH_3OH appearing in Orion at the velocity of the ambient material, but which seem to be more spatially confined. As this table shows, the abundances of nearly all of the simpler species are within factors of a few of each other, and certainly within a factor of 10, in the differing molecular clouds; and the abundances, for the most part, also seem to be reasonably well predicted by the purely gas phase ion-molecule networks of the type pioneered by Herbst and Klemperer (1973) and Prasad and Huntress (1980) that do not predict strong chemical variations from source to source with similar initial conditions. Gas phase ion-molecule chemistry would therefore appear to account for much of the chemical processing in quiescent, dense interstellar clouds.

It should be noted that most of the thousands of reaction rates used in such models have not been measured experimentally, and that considerable work remains before any definite conclusions about the dominance of gas phase chemistry can be reached. It would appear, however, that the abundances of

TABLE 4

MOLECULAR ABUNDANCES IN QUIESCENT CLOUDS

	ABUNDANCE RELATIVE TO H_2				
				Herbst and Leung[d]	
SPECIES	OMC-1[a]	Sgr B2[b]	TMC-1[c]	Model 1[e]	Model 2[f]
CO	5.0×10^{-5}	6.0×10^{-5}	5.8×10^{-5}	1.5×10^{-4}	3.4×10^{-4}
CN	3.3×10^{-9}	3.4×10^{-10}	3.0×10^{-8}	3.2×10^{-9}	2.4×10^{-5}
CS	2.5×10^{-9}	3.0×10^{-9}	2.0×10^{-9}	4.8×10^{-8}	1.5×10^{-7}
SO	$\lesssim 9.3 \times 10^{-10}$	1.5×10^{-10}	5.0×10^{-9}	1.2×10^{-8}	4.5×10^{-11}
SO_2	$< 3.3 \times 10^{-9}$	2.0×10^{-9}	...	4.8×10^{-8}	1.3×10^{-12}
C_2H	5.3×10^{-9}	...	8.4×10^{-9}	2.4×10^{-10}	2.7×10^{-6}
HCH	5.0×10^{-9}	$\sim 3.0 \times 10^{-9}$	1.2×10^{-8}	5.5×10^{-9}	1.0×10^{-6}
HNC	5.3×10^{-10}	$\sim 3.0 \times 10^{-9}$	8.0×10^{-9}	5.5×10^{-9}	1.0×10^{-6}
HCO^+	2.3×10^{-9}	2.3×10^{-9}	8.0×10^{-9}	1.0×10^{-8}	7.3×10^{-9}
HCS^+	5.3×10^{-11}	3.0×10^{-11}	5.0×10^{-10}	1.4×10^{-11}	5.3×10^{-11}
H_2D^+[g]	$\sim 1.0 \times 10^{-10}$	...	$< 3.0 \times 10^{-8}$	...	$\sim 1.1 \times 10^{-10}$
HC_3N	1.3×10^{-10}	3.8×10^{-10}	6.0×10^{-9}	3.5×10^{-12}	9.2×10^{-8}
HC_5N	$\lesssim 2.3 \times 10^{-11}$	...	1.0×10^{-8}	8.9×10^{-16}	6.2×10^{-10}
CH_3CN	3.2×10^{-10}	2.0×10^{-10}	5.0×10^{-10}	1.5×10^{-11}	8.5×10^{-8}
H_2CO	1.7×10^{-8}	3.0×10^{-9}	1.2×10^{-8}	7.7×10^{-9}	5.7×10^{-8}
CH_3OH	1.2×10^{-7}	2.0×10^{-8}	...	5.6×10^{-10}	1.6×10^{-8}

[a] Derived from this work and Johansson *et al.* 1984.
[b] Derived from Cummins, Linke, and Thaddeus 1986.
[c] From the data compilation in Leung, Herbst, and Huebner 1984.
[d] 1986.
[e] Model results for C/O = 0.4, $n_{\rm H_2} = 10^5$ cm^{-3}, $t = 10^7$ yr.
[f] Model results for C/O = 1.3, $n_{\rm H_2} = 10^5$ cm^{-3}, $t = 10^7$ yr.
[g] Abundances derived by Phillips *et al.* 1985.

most species are *not* strongly correlated with density, implying that some mechanism must exist to remove adsorbed molecules from grain surfaces deep within quiescent molecular clouds without significantly altering the composition of the gas. Several types of desorption mechanisms have been suggested ranging from grain mantle chemical explosions (d'Henecourt *et al.* 1982) to impulsive spot heating by X-rays and cosmic rays (Leger, Jura, and Omont 1985), but little is actually known which could differentiate between the various hypotheses.

Although the abundances in Table 4 are well predicted and rather similar for the various sources, there are also quite clearly a few sizable differences between the clouds and there are major failings in the chemical models, mostly related to the so-called "carbon problem" in dense molecular clouds (Phillips and Huggins 1981; Herbst 1983). For example, one sees that many carbon-rich species, particularly the higher cyanopolyacetylenes and the C_3N and C_4H radicals, have substantially greater abundances in TMC-1 than in either OMC-1 or Sgr B2. Moreover, the abundances of even simpler carbon-rich species such as C I, CN, HCS^+, or C_2H are sometimes vastly underestimated by models of evolved clouds under steady state conditions, and only somewhat better followed at intermediate time scales because of reactions of the type

$$C + O_2 \rightarrow CO + O\,, \quad (6)$$

$$CN + O \rightarrow CO + N\,, \quad (7)$$

which convert the carbon-rich species back into CO. Significant quantities of O I and O_2 are present in chemical models of dense interstellar clouds since the cosmic ratio of C/O = 0.4 leaves a considerable gas phase reservoir of oxygen even after reactions such as (6) and (7) convert reactive carbon-containing species like C I and CN into CO. In quiescent clouds such as the extended Orion ridge, the neutral-neutral reactions are not as fast as their ion-molecule counterparts, and it is for this reason that the predicted abundances of the carbon species noted above peak early in the cloud's evolution. Complicating this matter further in OMC-1 (and other clouds as well) is the presence of oxygen-rich species such as CH_3OH or $HCOOCH_3$ at similar velocities and positions to the carbon-rich molecules, but whose abundances are also underestimated by the models, especially those assuming C/O > 1. We defer a discussion of the large, oxygen-rich species to § V*d*, and concentrate here on the simpler carbon-rich compounds.

The species which illustrate the carbon problem in dense molecular clouds most dramatically are the neutral C I atom, first observed by Phillips *et al.* (1980), and the chemically related CCH radical. More extensive observations (Phillips and Huggins 1981; Keene *et al.* 1985; Frerking *et al.* 1986; Huggins, Carlson, and Kinney 1984) have shown that C I and CCH are widespread throughout molecular clouds and not simply restricted to the outer edges of these objects, in contrast to the predictions of early models. The inferred C I/CO ratio of 0.01–0.5 is nearly three orders of magnitude greater than even the most optimistic steady state predictions for the shielded cores of molecular clouds in which, as the preceding discussion shows, the conversion of C I → CO is expected to be essentially complete for cloud ages greater than $\sim 10^6$ yr. While it is difficult to accurately determine the ages of individual molecular clouds, observations of the distribution of these objects on a galactic scale suggests that their lifetimes are $\lesssim 10^8$ yr (Cohen *et al.* 1980). For large complexes like Orion the ages of stellar associations formed from the molecular gas may be used to establish lower bounds for the cloud lifetime, and are generally $\sim 10^7$ yr (Kutner *et al.* 1977). A number of new theories have been introduced since the observations of Phillips and Huggins (1981) which attempt to explain the large observed C I abundances by delaying the onset of *chemical* maturity in molecular clouds via a wide variety of processes. Keene *et al.* (1985) have recently summarized these models and have embarked on a series of observations designed to test their validity and observational consequences. Whether they utilize a delayed dynamical collapse of diffuse clouds into a set of denser fragments (Tarafdar *et al.* 1985), the convective transport of material deep within the cloud core to its unshielded outer edges (Boland and de Jong 1982), frequent mild shocking of the molecular cloud gas (Williams and Hartquist 1984), or the internal production of C I from CO via photodissociation by internal UV or X-ray sources (Prasad and Tarafdar 1983; Krolik and Kallman 1983), all such models assume that the available C I is in fact rapidly converted into CO and that some process must be found to "recycle" CO into the more reactive atomic species.

An alternative suggestion is that the *gas phase* C/O ratio in molecular clouds may vary considerably from its cosmic value of 0.4 (Langer *et al.* 1984). Obviously, if the gas phase C/O ratio is greater than unity in the cores of dense molecular clouds, then substantial amounts of C I and other carbon-rich species may remain long after all of the available gas phase oxygen has been locked away in CO. The major difficulty with this approach is that it now becomes difficult to reproduce the observed abundances of the oxygen-containing molecules such as CH_3OH, but it does have a number of supporting observations and theoretical predictions. In addition to the high abundances of C I, CN, and C_2H, Prasad and Huntress (1982) also conclude from their theoretical study of sulfur in dense molecular clouds that the observed chemistry of this family is inconsistent with an undepleted gas phase oxygen concentration. Specifically, they use the observed SO abundance and the HCS^+/CS ratio to conclude that $f(O) \lesssim 6 \times 10^{-7}$, well below its predicted (undepleted) value of $4\text{–}5 \times 10^{-5}$. Further, both Herbst (1983) and Leung, Herbst, and Heubner (1984) require a large C I content in the cores of dense clouds in order to reproduce the observed hydrocarbon abundances in many sources, particularly in the dark, truly quiescent clouds like TMC-1 and L183 which do not appear to contain easily detectable amounts of oxygen-rich molecules like $HCOOCH_3$ or CH_3OCH_3. As Table 4 shows, the carbon-enriched model overproduces many carbon-containing species at steady state, while the previous models predict considerably lower abundances than are actually observed, suggesting that the oxygen depletion lies somewhere in between these limiting extremes.

That some selective depletion mechanism is required to increase the C/O gas phase ratio to values greater than unity is clear. While the first-row elements appear to be depleted by no more than factors of 10–100, the observations of several Si or S-containing species are most consistent with depletions in the range of 1000 (Prasad and Huntress 1982), supporting the intuitively appealing hypothesis that the more refractory elements and molecular species should be the most strongly depleted. Could such a mechanism explain a high gas phase C/O ratio? Early in the lifetimes of molecular clouds most species, with the exception of H_2, are primarily neutral and atomic. Consider a scenario in which C I, N I and O I collide with grains and stick to them with equal probabilities. Once residing on the grain surface, the chemically active H/H_2 mantle thought to cover

most grains (Allen and Robinson 1977; Tielens and Hagen 1982) will proceed to hydrogenate these species until the fully hydrogenated end products, CH_4, NH_3, and H_2O, are formed. Of these, CH_4 will most easily evaporate from the cold grain surfaces due to its nonpolar nature. Indeed, the sublimation temperatures of pure ammonia or water mantles are well above 150 K, and such ices will remain frozen onto grain surfaces in all but the warmest regions of molecular clouds. Observational support for the existence of a substantial molecular grain mantle stems mainly from the study of several infrared features near 3.0, 3.1, 4.6, and 6.0 μm, observed in absorption against deeply embedded sources, which have been identified as the stretching bands of a "dirty ice" layer composed mainly of H_2O and NH_3, with smaller concentrations of CO, H_2CO, etc. The 3.8 μm bands are best fitted by a $4(\pm 1):1$ mixture of $H_2O:NH_3$ and indicate that the fractional abundance of H_2O and NH_3 on the grain mantles exceeds 10^{-5} (Knacke *et al.* 1982; Whittet *et al.* 1983). In addition, searches for gas-phase H_2O, which is predicted to be quite abundant by the standard ion-molecule chemical models, have failed to detect H_2O in quiescent clouds, but have shown instead that water emission may be a good tracer of the sometimes violent activity associated with star formation.

Thus, it would appear that there are mechanisms available which could significantly enhance the gas phase C/O ratio in quiescent molecular clouds leading to the high carbon abundance detected there. A major step forward in the verification of this hypothesis would be the identification of CH_4 in the cores of quiescent molecular clouds since it is predicted to be a major reservoir of carbon in a carbon-rich gas (Watt 1985). Unfortunately, it possesses no permanent dipole moment, and any study of CH_4 must rely on its infrared absorption spectrum toward bright, embedded sources around which the expected depletion is small. In spite of the above difficulties, it is concluded, for the most part, that the time-dependent ion-molecule reaction networks described above can account both qualitatively and quantitatively for the simpler aspects of the chemical composition now well characterized in a number of sources, although the initial cloud composition and its subsequent chemical evolution may be selectively influenced by grain depletion processes.

b) The Plateau Source

In contrast to the relatively well-understood composition of the extended Orion molecular cloud, the abundances of various species in the plateau source have been interpreted as resulting from a wide variety of processes, all related to outflow driven by IRc 2. The basic difference in the chemistry of the ridge and the plateau sources is that the passage of shock waves in the latter, and the concomitant temperature increase, make the high-activation neutral-neutral reactions more important. Some molecules have their abundances markedly enhanced or reduced, while others remain nearly unchanged relative to the ambient cloud. A pictorial representation of the differing chemistry in the plateau and ridge sources is presented in Figure 4, which depicts the $^{13}CO/SO$ abundance ratio as a function of radial velocity and which also illustrates the method used in §§ II and III to determine the plateau fractional abundances. As one can see, the SO abundance relative to CO increases sharply away from velocities characterizing the quiescent ridge clouds, but is roughly constant in the region with $\delta v \gtrsim 20$ km s^{-1} (δv = velocity offset from line center).

By performing such analyses on the many species found to exhibit high-velocity emission, the overall plateau chemical composition shown graphically in Figure 5 has been established, from which a number of general conclusions may be

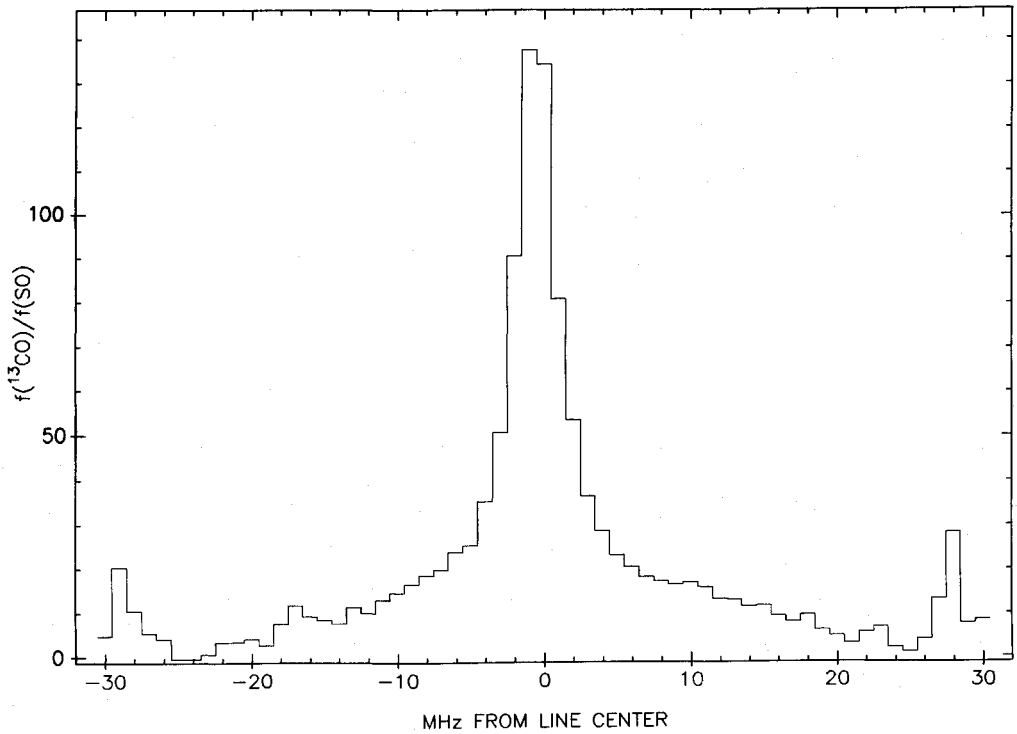

FIG. 4.—CO/SO abundance as a function of offset frequency (1 MHz equals ~ 1.3 km s^{-1}), illustrating the potentially large enhancements in sulfur compound relative abundances observed in the plateau.

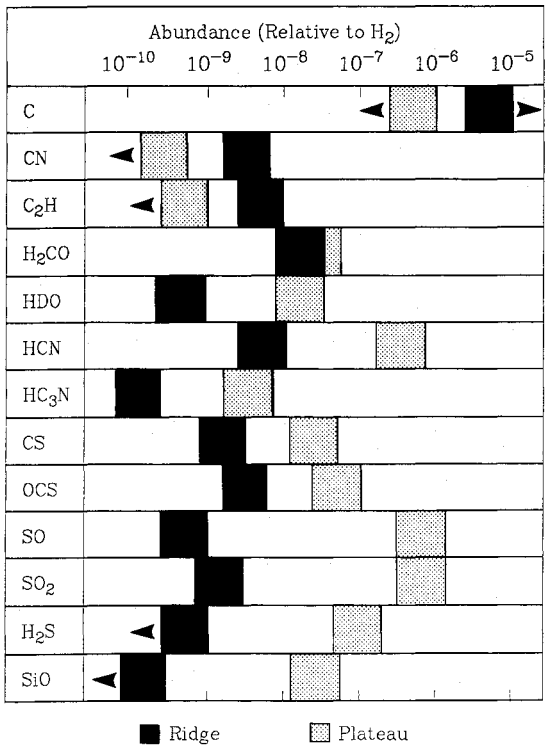

FIG. 5.—Graphical comparison of the OMC-1 ridge and plateau fractional abundances.

drawn. Emission from the reactive C I, CN, and C_2H species so prominent in the ambient gas is now undetectable, while the abundances of several oxygen-rich species like SiO, SO, and SO_2 are considerably enhanced. Unlike the ambient cloud chemistry, the plateau composition is most consistent with a region in which the gas phase C/O ratio is normal or low, as would be expected for an outflow from young, oxygen-rich stars or for rapid desorption from grains. Further support for this hypothesis is provided by the observations of O I and CO in the high-velocity shocked material surrounding the plateau source. Werner *et al.* (1984) conclude that if the [O I] 63.2 μm emission arises in the warm, postshocked gas, the abundance of O I is at least 10^{-4}. For CO, Watson *et al.* (1985) find that $CO/H_2 = 0.8\text{–}1.5 \times 10^{-4}$ in the warm, postshock gas. An even higher CO fractional abundance ($CO/H_2 \approx 5.5 \times 10^{-4}$) has been derived by Scoville *et al.* (1983), who infer from high-resolution 4.6 μm infrared observations toward BN that all of the available carbon in the gas phase is in the form of CO. The estimated O I abundance is particularly high, and leads to a number of enhancements in other species.

Most dramatically enhanced are the silicon and sulfur species SiO, SO, SO_2, and H_2S whose relative abundances are greater than those in the quiescent gas by factors exceeding 100 (see Figs. 4 and 5). HDO, HCN, and HC_3N are enhanced by somewhat smaller amounts, while species such as CS, OCS, and H_2CO are only slightly enhanced. The low CS enhancement is further indication of a high gas-phase oxygen abundance in the plateau because, unlike SiO, OCS, or H_2S, it reacts rapidly with O I:

$$CS + O \rightarrow CO + S ,$$

forming CO. The high sulfur abundances in the plateau have been interpreted by a number of authors as evidence for a shock-induced chemistry (Iglesias and Silk 1978; Hartquist, Oppenheimer, and Dalgarno 1980; Dalgarno 1982). That shocks exist in Orion is clear from the observations of vibrationally excited H_2 and far-infrared high-J CO emission. The apparent absence of hot gas in the "low-velocity" (18 km s^{-1}) outflow may simply be due to sensitivity and other observational effects, since the high density in this source will rapidly cool the postshocked region resulting in a very thin shock front with little column density. The chemical modifications arising from a propagating shock front last much longer (Igesias and Silk 1978), but it is not clear from the observed chemistry that shocks have affected the bulk of the material in the 18 km s^{-1} outflow. Some species must clearly be formed very close to IRc 2 in a presumably less turbulent, high-temperature outflow more characteristic of circumstellar shells, as is illustrated by the SiO masers which lie only 70 AU from IRc 2 (Wright and Plambeck 1983). Further, the high fractional abundances of fragile species like HDO and H_2CO, which could not survive the passage of a strong shock front nor which would be created in significant amounts in the postshock medium, illustrate that a significant fraction of the outflow material is contained in high-density clumps whose composition is not greatly altered from their initial states (Wootten, Loren, and Bally 1984). The plateau HDO content is a particularly good indication of density inhomogeneities, for although the expected shock-induced H_2O abundance is extremely high [$f(H_2O) \approx 2 \times 10^{-4}$], the degree of deuterium fractionation in the high-temperature postshocked molecular gas should be negligible, giving a predicted HDO abundance of $f(HDO) \lesssim 10^{-9}$, well below the observed value.

Prasad and Huntress (1982) have shown, moreover, that if one simply assumes a smaller depletion of the heavier elements, then "standard" ion-molecule and neutral-neutral reaction networks can account for much of the observed sulfur chemistry. A comparison of the shock-induced chemical models with the results from Prasad and Huntress, which assume a gas-phase oxygen content of $f(O) \approx 5.5 \times 10^{-5}$ and a sulfur depletion of 10 [$f(\Sigma S) \approx 1.7 \times 10^{-6}$], is presented in Table 5. The model of Hartquist, Oppenheimer, and Dalgarno (1980) has been used for the oxygen and sulfur high-temperature shock chemistry, while the results of Iglesias and Silk (1978) have been used for the remaining species. For the simpler molecules CS, SO, and OCS the models are nearly identical, but

TABLE 5

THEORETICAL PREDICTIONS OF THE SHOCKED AND QUIESCENT CLOUD MODELS

SPECIES	ABUNDANCE RELATIVE TO H_2		
	Shocked[a]	Quiescent[b]	Observed
CS	4.7×10^{-8}	3.9×10^{-8}	2.2×10^{-8}
OCS	1.6×10^{-7}	2.4×10^{-8}	5.2×10^{-8}
SO	3.7×10^{-8}	5.5×10^{-7}	5.2×10^{-7}
SO_2	3.7×10^{-11}	8.8×10^{-7}	5.2×10^{-7}
H_2S	4.0×10^{-7}	2.3×10^{-9}	9.8×10^{-8}
SiO	2.5×10^{-8}	...	2.8×10^{-8}
HCN	2.0×10^{-8}	2.3×10^{-9}	2.8×10^{-7}
H_2O	2.0×10^{-4}	2.0×10^{-6}	$\lesssim 1.7 \times 10^{-5}$
H_2CO	$< 1.0 \times 10^{-11}$	2.0×10^{-9}	3.1×10^{-8}

Typical carbon star circumstellar abundances:
$f(H_2S) = 5.3 \times 10^{-7}$ $f(SiO) = \lesssim 6.0 \times 10^{-7}$ $f(HCN) = 1.1 \times 10^{-5}$

[a] Hartquist, Oppenheimer, and Dalgarno 1980.
[b] Prasad and Huntress 1982.

major differences arise in the predicted abundances of HCN, H_2O, H_2S, and SO_2. In the quiescent cloud model all reactions which initiate the formation of H_2S, unlike those for H_2O, are quite endothermic, and its predicted abundance is therefore rather low. The high kinetic temperatures associated with the postshocked gas easily overcome such endothermicity barriers, however, and the great thermodynamic stability of H_2S leads to the large predicted hydrogen sulfide abundance in the shock models. Similarly, the endothermic reaction

$$H_2 + CN \rightarrow HCN + H$$

is quite rapid in the hot, shocked regions and is primarily responsible for the decreased CN and increased HCN abundances, but is negligible in the time-dependent cold cloud models. Conversely, the shock models produce too little SO_2 because of the high O I abundance and the reaction

$$SO_2 + O \rightarrow SO + O_2 ,$$

while the standard cloud models reproduce the observed SO/SO_2 ratio extremely well. The (highly uncertain) observed H_2O abundance of $\sim 2 \times 10^{-5}$ (Phillips, Kwan, and Huggins 1980) lies between the upper and lower limits defined by the shock and cloud chemistry models, and the resulting fractionation ratio of $f(H_2O)/f(HDO) \approx 1000$ (compared to the extended cloud value of ~ 100) suggests that the outflow material is strongly clumped.

Also listed in Table 5 are the abundances found in circumstellar shells for the HCN, H_2S, and SiO species not well predicted by the cloud model. As these values show, a combination of high-temperature chemistry in the initial outflow close to the star with lower temperature ion-molecule and neutral-neutral processing of the dense gas in the outer outflow can mimic the large enhancements found in most shock models. It should also be noted that the SO_2 abundance in the shock models could be substantially increased by the inclusion of a stellar outflow chemistry. Little is actually known about the composition of circumstellar shells around oxygen-rich stars, and a general spectral line survey of such objects may yield a great deal of useful information on the contribution of circumstellar chemistry to the observed composition of the plateau source. Perhaps, then, the most plausible scenario is one in which outflow from IRc 2 produces species like the SiO and OH or H_2O, which are manifest as masers immediately surrounding the star, while simultaneously accelerating the gas, raising its temperature, and disrupting some of the smaller dust grains to liberate the more refractory elements such as silicon and sulfur. As the outflow expands into the partially evacuated cavity enveloping IRc 2, chemical reactions in the gas and in the shock fronts created where the outflow strikes the dense cavity walls produce the high observed abundances of SO, SO_2, HCN, H_2O, etc. Embedded in the outflow are dense clumps of gas and dust containing molecules such as HDO, H_2CO, and HC_3N. The temperature in these clumps is sufficient to release most molecules from the grain surfaces on which they condensed but not to destroy them, thereby offsetting the destruction of such species in the shocked regions of the less dense material.

c) *The Hot Core*

The crucial nature of gas-grain interactions to the chemistry of dense molecular clouds is perhaps most easily recognized in the hot core region of Orion. Radiative heating from the luminous IRc 2 source passively induces gas and grain temperatures of $\gtrsim 150$–300 K, more than sufficient to release even the most tightly bound grain mantle constituents such as H_2O and NH_3. The high density and temperature of the hot core leads to a low fractional ionization of the gas and therefore "shuts down" the ion-molecule reaction networks while increasing the importance of neutral-neutral processes. Any initial mixture of gas phase and grain produced species will therefore be driven rapidly toward kinetic equilibrium with the abundances of the most reactive species markedly reduced. As the preceeding discussion showed, the evaporation of grain mantles will return the gas phase C/O ratio to near its cosmic value, thereby producing an oxygen-rich environment.

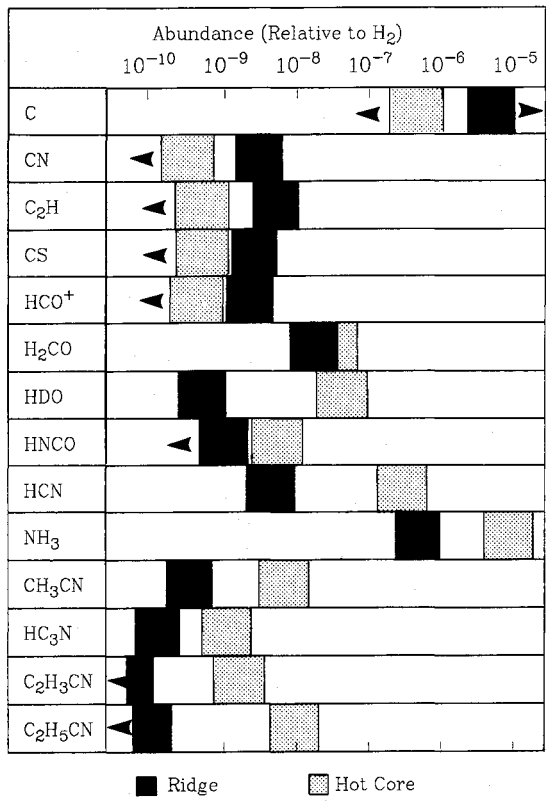

FIG. 6.—Graphical comparison of the OMC-1 ridge and hot core fractional abundances.

The observed hot core chemical composition summarized graphically in Figure 6 is, generally, consistent with the hypothesis that grain mantle evaporation and kinetic equilibrium dominate chemistry in the hot core. Just as in the plateau source the abundances of reactive carbon-rich species like C I, CS, CN, and C_2H are dramatically suppressed, while the CO abundance is enhanced relative to the quiescent ridge clouds, indicating a high gas-phase oxygen content. However, the oxygen-rich species SiO, SO, and SO_2, which dominate the plateau chemistry, are not clearly detectable, but instead nitrogen-containing compounds such as HCN and NH_3 are very abundant. Where is the remaining oxygen? An analysis of the expected grain mantle composition provides some clues. Tielens and Hagen (1982) have calculated the molecular composition of absorbed grain mantles under a wide variety of conditions. Their results, presented in Table 6 along with some observed hot core abundances, show that the final mantle composition depends sensitively on the nature of the accreting species. The two predicted abundance columns in Table 6 cor-

TABLE 6

PREDICTED GRAIN MANTLE COMPOSITIONS AND OBSERVED HOT CORE ABUNDANCES

Species	"Cosmic"	ζ Oph	Observed
N_2	1.1×10^{-5}	3.7×10^{-6}	...
O_2	1.4×10^{-7}	5.0×10^{-7}	$<1.0 \times 10^{-4}$ [a]
CO	5.6×10^{-6}	1.7×10^{-7}	1.2×10^{-4}
H_2O	8.3×10^{-6}	4.0×10^{-5}	$\gtrsim 5.3 \times 10^{-6}$
CO_2	1.1×10^{-4}	3.6×10^{-6}	$<1.0 \times 10^{-5}$ [b]
H_2CO	1.5×10^{-5}	1.7×10^{-5}	2.6×10^{-8}
NH_3	1.0×10^{-5}	4.8×10^{-7}	1.0×10^{-5}
CH_4	1.6×10^{-5}	2.7×10^{-9}	$<1.0 \times 10^{-5}$ [c]
H_2O_2	8.2×10^{-8}	1.4×10^{-6}	$<4.5 \times 10^{-10}$

[a] From the $^{16}O^{18}O$ $N = 2 \rightarrow 0, J = 1 \rightarrow 1$ line at 233, 946 MHz.
[b] Inferred from the related $HOCO^+$ ion.
[c] Upper limit from CH_3D.

respond to a set of undepleted cosmic elemental abundances and a set of depleted abundances as observed toward ζ Oph, and have been normalized using the 3.1 μm ice band absorption spectra of Knacke *et al.* (1982). The predicted abundances demonstrate that, as expected, the grain mantle is oxygen rich.

If, as Tielens and Hagen assume, most of the carbon and nitrogen adsorbed onto the grain mantle is molecular in form, then the unobservable species CO_2 would contain the bulk of both the carbon and oxygen in the hot core. However, if a significant atomic population initially resides on the grains, then H_2O, NH_3, and CH_4 are the dominant mantle constituents. The H_2O hot core abundance must be estimated from the detected HDO species, and uncertainties in the residual fractionation introduce large errors into its estimated concentration. A lower bound of $f(H_2O) > 3 \times 10^{-6}$ is provided by the large fractionation observed in the HCN/DCN ratio in the hot core, while the deuterium fractionation observed in the plateau source gives an H_2O fractional abundance of $f(H_2O) \gtrsim 5 \times 10^{-5}$ or higher (Olofsson 1984). The large inferred values of $f(H_2O)$ and $f(NH_3)$ are more consistent with an initially atomic grain mantle composition, as is the low observed enhancement of the H_2CO abundance in the hot core and the quiescent cloud chemistry discussed earlier. In either case, the dominant oxygen carrier (CO_2 or H_2O) is relatively chemically inert and only observable with great difficulty. The O I abundance may also be appreciable, but the spectral and spatial resolution of present far-IR instruments is insufficient to separate the hot core from the strong foreground emission arising in the photodissociation region between M42 and OMC-1. Thus, nitrogen-containing species like HCN, HC_3N, and NH_3, that are so readily observable at millimeter wavelengths because of their simple rotational spectra and large dipole moments, dominate the spectral appearance of the hot core. Oxygen-rich sulfur species such as SO or SO_2 are not observed in the hot core because its passively achieved temperature, while high enough to liberate the grain mantles, is insufficient to disrupt the highly refractory grain cores which are thought to contain most of the heavier elements like Si or S.

The abundances of several hot core species, particularly H_2O and NH_3, are well-matched by models incorporating complete evaporation of grain mantles, and are indicative of the high efficiency of hydrogenation of grain surfaces (Sweitzer 1978). For example, in their analysis of the 3.1 μm water ice bands observed toward TMC-1, Jones and Williams (1984) conclude that the conversion of $O \rightarrow H_2O$ on grain surfaces has an efficiency of greater than 70%. One might therefore expect fully hydrogenated, or saturated, species to dominate the hot core chemistry, and, as Figure 5 shows, they do. The abundances of HCN, NH_3, CH_3CN, C_2H_5CN, and HDO are all markedly higher in the hot core than in the quiescent clouds. The C_2H_3CN and C_2H_5CN molecules are most naturally explained by a grain surface production mechanism as gas phase reactions like

$$HC_3NH^+ + H_2 \rightarrow C_2H_3CN^+ + H\,,$$

$$C_2H_3CN^+ + H_2 \rightarrow C_2H_4CN^+ + H\,, \quad \text{etc.}\,,$$

are highly endothermic and proceed quite slowly (Herbst, Adams, and Smith 1983), while the hydrogenation of cyanoacetylene on grain surfaces should be fairly efficient. The fact that C_2H_3CN and C_2H_5CN are observed only in the hot core is further indication that they originate on grain surfaces, since only the hot core has temperatures that are sufficient to release them from the grain mantles. The observed ratios of $f(HC_3N/C_2H_3CN)$ and $f(HC_3N/C_2H_5CN)$ in the ridge and hot core sources suggest that the hydrogenation process prefers to saturate any cyanoacetylene deposited on the grain surface completely, and that the conversion efficiency is on the order of 25%–75%.

From the abundances of chemically stable molecules such as HCN, H_2CO, and CH_3CN which are found in both the ridge and hot core components, limits may be placed on the degree of carbon and oxygen depletion in the cool, quiescent gas. The observed ratios suggest that the depletion of most simple carbon-rich species is not greater than a factor of 10 in the ridge clouds near Orion-KL. The oxygen depletion is more difficult to assess because of the difficulty or impossibility of observing H_2O and CO_2, but it would appear to be much greater than the carbon depletion from observed abundances of HDO. These conclusions confirm the necessity for some mechanism which could remove molecules selectively from grain surfaces, but do not in any way constrain the possible alternatives.

d) The Compact Ridge Source

Yet another example of the chemical selectivity in OMC-1 is provided by the compact ridge source in which most of the large, oxygen-rich molecules found in Orion have their maximum abundance. The high HDO content of this source and the presence of other species such as SO and OCS strongly suggest that the compact ridge has been created by an interaction between outflowing material from the plateau and the quiescent 8 km s^{-1} cloud (see § III). Such an interaction would release the large gas-phase oxygen abundance required in the compact ridge. Carbon-rich species such as HCN or HC_3N are also undoubtedly present, but their extended emission "masks" any contribution from the more compact source. Since the oxygen-rich species do not appear to have an extended counterpart, they stand out more clearly to produce the spectral signature of the compact ridge source.

As an illustration of the unique chemistry of the compact ridge, Table 7 presents a comparison of the abundances found in this region with those observed in another source of oxygen-rich molecules, Sgr B2 (Cummins, Linke, and Thaddeus 1985), and with the theoretical predictions of Leung, Herbst, and Huebner (1984). This comparison shows that the enhancements observed in the abundances of complex molecules in the compact ridge are not uniform but are, in fact, rather selective.

TABLE 7

MOLECULAR ABUNDANCES IN THE ORION COMPACT RIDGE AND SGR B2

Species	OMC-1	Sgr B2	Leung, Herbst, and Huebner[a]	Steady State
CH_3CN	3.2×10^{-10}	2.0×10^{-10}	8.1×10^{-10}	1.0×10^{-9}
HCOOH	5.0×10^{-10}	1.0×10^{-10}	4.6×10^{-9}	4.0×10^{-9}
CH_3CHO	$\lesssim 1.7 \times 10^{-10}$	2.0×10^{-10}	2.1×10^{-10}	1.0×10^{-11}
C_2H_5OH	$< 5.0 \times 10^{-10}$	7.5×10^{-10}	4.1×10^{-11}	1.0×10^{-10}
H_2CO	1.7×10^{-8}	3.0×10^{-9}	1.5×10^{-8}	5.0×10^{-8}
CH_3OH	1.2×10^{-7}	3.1×10^{-8}	1.8×10^{-9}	2.0×10^{-7}
$HCOOCH_3$	8.7×10^{-9}	3.4×10^{-10}	1.0×10^{-11}	3.0×10^{-9}
CH_3OCH_3	1.0×10^{-8}	5.0×10^{-10}	1.9×10^{-11}	1.3×10^{-8}

[a] 1984.

Apparently simple species such as HCOOH and CH_3CHO have similar abundances in the two clouds and are well predicted theoretically, but other species like CH_3OCH_3 or $HCOOCH_3$ are significantly enhanced relative to other regions in Orion, Sgr B2, and the model predictions. Further, neither C_2H_5OH nor CH_3COOH has been detected in OMC-1, while their structural isomers CH_3OCH_3 and $HCOOCH_3$ are quite abundant. Thus, the mechanism which drives the oxygen chemistry in the compact ridge must be fundamentally different from those processes operating in the plateau or hot core regions, particularly in its selectivity and in its ability to produce complex molecular species.

The very nature of the large molecules found in the compact ridge provides the key to an understanding of both the enhancement process and its chemical selectivity. As Herbst and Klemperer (1973), Huntress and Mitchell (1979), and Leung, Herbst, and Huebner (1984) have shown in their pioneering calculations, the most efficient formation routes to complex interstellar species are via radiative association reactions of the type

$$A^+ + B \rightarrow AB^+ + h\nu \,. \qquad (8)$$

Radiative asociation reactions involving purely neutral reactants are considerably slower than the ion-molecule radiative association process depicted in equation (8) because the neutral-neutral intermediate complex has a much shorter lifetime in which to stabilize itself radiatively. In addition, the spontaneous emission rates of even quite simple molecular ions appear to be significantly greater than their neutral counterparts, and such ions are therefore more easily stabilized radiatively (Herbst 1985). The rates of ion-molecule radiative association reactions are particularly sensitive to temperature with a dependence of $T^{-(r_{A^+}+r_B)/2}$, provided the rotational state quantization may be ignored, where r_{A^+} and r_B are the rotational degrees of freedom of the reacting fragments. Regions with high temperatures or a small fractional ionization, such as the plateau and hot-core components, do not therefore favor the production of large, complex molecules by radiative association reaction pathways. The lower temperature and intermediate density of the compact ridge is such, however, that radiative association reactions should still proceed rapidly. Combined with the increased oxygen content available from material introduced by the interaction with the outflow source, such reactions may be able to account for the high abundances and the remarkable degree of chemical selectivity found in the compact ridge.

Table 8 presents a listing of some of the most important radiative association reactions found in the model of Leung, Herbst, and Huebner (1984), and later reevaluated by Herbst (1986), for a kinetic temperature of 10 K. Uncertainties in the reaction rates are difficult to estimate, but a recent measurement of the $CH_3^+ + H_2$ reaction yielded a value of ~ 5 times the predicted rate constant (Barlow, Dunn, and Schauer 1984), and the rates listed in Table 8 should provide useful lower bounds (Herbst 1985, 1986). The CH_3^+ ion is a particularly suitable partner in radiative association reactions as is evidenced by its rapid predicted reactions with HCN and H_2O, the products of which ultimately produce CH_3CN and CH_3OH. Because of the high HCN and H_2O abundances in the outflow and the prominence of CH_3^+ in the ion-molecule models of interstellar chemistry (Prasad and Huntress 1980; Leung, Herbst, and Huebner 1984), these reactions should substantially increase the abundances of both CH_3CN and CH_3OH. From the estimated reaction rates and the observed plateau fractional abundances a simple algebraic calculation predicts that $f(CH_3CN) \approx 10^{-9}$ and $f(CH_3OH) \approx 10^{-7}$, in good agreement with the estimated compact ridge composition. The enhancement time scales of $\gtrsim 100$ yr are substantially less than the inferred outflow age of 1000 yr. In contrast, the reaction rates leading to the formation of HCOOH, CH_3CHO, and C_2H_5OH are considerably slower (the $C_2H_5^+$ ion is substantially less abundant than CH_3^+), and even though HCO^+, H_2O, and CH_4 are quite abundant, the expected enhancement time is $\gtrsim 1000$ yr. Thus, one expects CH_3CN and CH_3OH to have enhanced abundances while HCOOH, CH_3CHO, and C_2H_5OH should not be greatly affected, as is observed.

What of the other species observed in the condensed ridge? Except for H_2CO, most of these species are characterized by a CH_3O-X structure and are intimately related chemically, as Figure 7 shows. The initial production of $CH_3OH_2^+$ from the radiative association of CH_3^+ and H_2O eventually leads to a number of other species. Except for this reaction and the interaction of $CH_3OH_2^+$ with H_2CO, all of the channels presented

TABLE 8

ESTIMATED RADIATIVE ASSOCIATION REACTION RATES AT 10 K

Reaction	Rate ($cm^3\ s^{-1}$)
$CH_3^+ + HCN \rightarrow CH_3CNH^+$	4.9×10^{-8}
$CH_3^+ + H_2O \rightarrow CH_3OH_2^+$	3.6×10^{-10}
$C_2H_5^+ + H_2O \rightarrow C_2H_5OH_2^+$	4.7×10^{-10}
$HCO^+ + H_2O \rightarrow H_2COOH^+$	6.7×10^{-12}
$HCO^+ + CH_4 \rightarrow CH_3CHOH^+$	1.0×10^{-14}

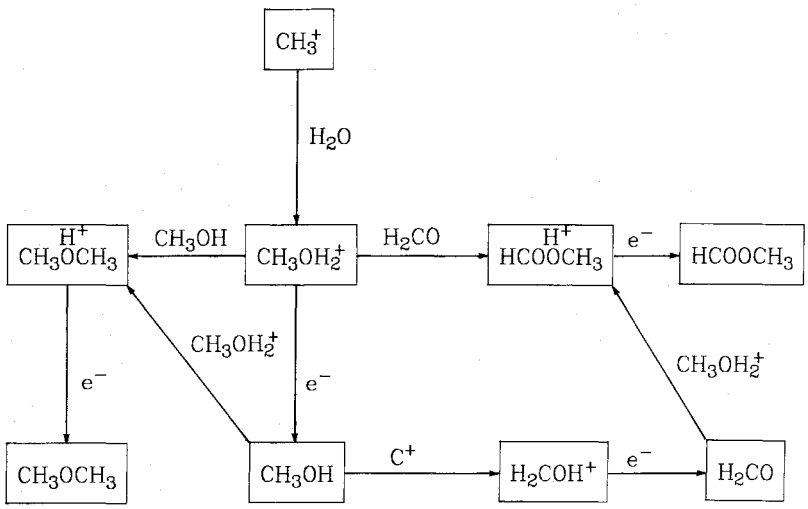

FIG. 7.—Pictorial outline of the steady state chemistry used to model the oxygen-based compact ridge abundances

in Figure 7 are well understood. Reactions of the abundant CH_3OH and H_2CO neutral molecules with $CH_3OH_2^+$ selectively produce the ionic precursors to CH_3OCH_3 and $HCOOCH_3$, whose structures are shown in Figure 7. The creation of $C_2H_5OH_2^+$ or $CH_3COOH_2^+$ ions from the dimerization of methanol or the reaction of $CH_3OH_2^+$ with H_2CO would clearly require a great deal of structural rearrangement, and the reaction probabilities are correspondingly low. Reactions with the abundant C^+ ion, such as that which produces H_2CO from CH_3OH, are not shown in Figure 7 but are the dominant loss channels of CH_3OCH_3 and $HCOOCH_3$, and lead back to CH_3OH. Thus, the H_2CO, CH_3OH, CH_3OCH_3, and $HCOOCH_3$ species are connected to each other chemically and will be similarly enhanced, while neither C_2H_5OH nor CH_3COOH will be produced.

A steady-state analysis of the reaction network outlined in Figure 7 is presented in Table 7 which quantitatively reflects the hypothesized enhancement process. If, as we have assumed, the recombination reactions of the precursor ions with electrons and the reactions of C^+ with the neutral species proceed at the same rates k_e and k_{C^+} (Huntress 1977), then the steady-state model leads to a number of very simple relationships between the abundances of the X–OCH_3 family. Specifically, we find that

$$\frac{[H_2CO]}{[CH_3OH]} = R\,, \tag{9a}$$

$$\frac{[HCOOCH_3]}{[CH_3OCH_3]} = \frac{[H_2CO]}{[CH_3OH]}\,, \tag{9b}$$

$$\frac{[CH_3OH]}{[CH_3OCH_3]} = \frac{k_e[e]}{k_{CH_3OH_2^+}[CH_3OH]}\,, \tag{9c}$$

where R is the branching ratio of the electron recombination reaction

$$H_2COH^+ + e^- \xrightarrow{R} H_2CO + H \tag{10a}$$

$$H_2COH^+ + e^- \xrightarrow{1-R} HCO + H_2 \tag{10b}$$

and k_e and $k_{CH_3OH_2^+}$ are the rate constants of the reactions of $CH_3OH_2^+$ with electrons and CH_3OH:

$$CH_3OH_2^+ + e^- \xrightarrow{k_e} CH_3OH + H\,,$$

$$CH_3OH_2^+ + CH_3OH \xrightarrow{k_{CH_3OH_2^+}} CH_3OCH_4^+ + H_2\,.$$

As Table 7 shows, the predicted abundances generally reproduce the observed abundances to within factors of 2–5. In particular, this simple model correctly predicts the ratio of CH_3OH to its heavier analogs $HCOOCH_3$ and CH_3OCH_3. The observed H_2CO/CH_3OH ratio implies that $R \leq 0.2$, where the upper limit arises because H_2CO also produced by the reaction of CH_3 with O I:

$$CH_3 + O \rightarrow H_2CO + H\,.$$

This reaction has not been included in the steady state model, but the high O I abundance in the plateau gas should make it a major source of formaldehyde. The greatest discrepancy between the observed and calculated abundances occurs for HCOOH, which the model predicts to be nearly as abundant as either $HCOOCH_3$ or CH_3OCH_3. Presumably this results from an overoptimistic value of the rate constant for the radiative association reaction that forms the ionic precursor to HCOOH (Table 4.10), since the abundances of the HCO^+ and H_2O reactants are known to be high.

The abundances of CH_3OH, CH_3OCH_3, and $HCOOCH_3$ in Sgr B2, while lower than those detected in Orion, are still considerably higher than predicted by the model of Leung, Herbst, and Huebner (1984), and may indicate that similar processes operate in other giant molecular clouds in which embedded sources and molecular outflows are regularly observed. Orion may be somewhat special in that it contains a strong shock which produces considerable quantities of H_2O, but milder versions of the Orion outflow should also maintain a high gas-phase oxygen abundance in the active cores of other giant molecular clouds.

VI. SUMMARY

By combining a dedicated millimeter-wave spectral line survey with selective laboratory observations of important internal rotors, it has been possible to investigate the chemical

composition of the Orion molecular cloud in considerable detail. Specifically, over 800 individual features from 29 distinct species have been identified, dramatically illustrating the usefulness of molecular rotational line emission in determining the chemical and physical nature of the interstellar medium. The emission from Orion is clearly resolvable into at least four distinct subsources whose chemical compositions differ markedly from each other:

1. The cool and extended quiescent ridge gas is characterized by fairly simple carbon-rich species such as CN, C_2H, and C_3H_2 whose abundances are similar to that found in other well-studied objects like TMC-1 and Sgr B2. Its chemical composition is reasonably well predicted by purely gas phase ion-molecule reaction networks, although the relative constancy of the observed abundances in various objects and the low inferred gas-phase oxygen content may be indicative of selective grain adsorption and desorption mechanisms.

2. Abundances in the high-velocity plateau source are dominated, as expected, by outflow from IRc 2. Shock-induced chemistry plays a role in the production of the highly enhanced abundances of the silicon and sulfur molecules SiO, SO, SO_2, and H_2S observed predominantly in this source, but the relative contributions of a more organized and quiescent high-temperature circumstellar outflow or cloud embedded chemistry may also be substantial. The significant fractional abundances of fragile species such as HDO and H_2CO, which could not survive the passage of a strong shock front, imply that the density structure of the outflow is quite inhomogeneous; and that even if shocks are prevalent, they do not process all of the material involved in the outflow from IRc 2.

3. The hot core is interpreted as a particularly large and dense clump, or clumps, of gas left over from the formation of IRc 2 which has (have) yet to be dispersed by the supersonic outflow. Its close proximity to IRc 2 accounts for its high density and temperature, which are sufficient to shut down the ion-molecule reaction networks and release the material adsorbed onto grain mantles. At such high temperatures neutral-neutral reactions become important and drive the chemistry toward kinetic equilibrium. Most of the oxygen in this source is tied up in the currently unobservable O I, H_2O, or CO_2 species, and easily detected nitrogen-rich compounds like NH_3 or CH_3CN therefore dominate its spectral appearance. Significant processing of the atoms and molecules adsorbed onto the grain mantles may have occurred, as is evidenced by the prevalence of fully hydrogenated species such as H_2O, HCN, NH_3, CH_3CN, and C_2H_5CN in the hot core as compared with the rest of the Orion molecular cloud.

4. Finally, the production of complex oxygen-rich species such as CH_3OH in the compact ridge, which is formed by the interaction of the plateau source with the ambient molecular cloud, is accomplished via radiation association reactions between smaller molecular ions in the quiescent cloud material and highly abundant neutral species such as HCN and H_2O supplied by the outflow from IRc 2. The reaction between CH_3^+ and H_2O is particularly important since it leads to enhanced abundances of H_2CO, CH_3OH, CH_3OCH_3, and $HCOOCH_3$. A highly selective chemical composition is maintained in the compact ridge by the greatly different rates of the ion-molecule radiative association reactions which initiate the formation sequences of the complex molecules. Other species similar to to those found in the extended ridge cloud are also present, but the observed contrast is highest for the large oxygen-rich species because they are produced most efficiently in the compact ridge, thereby providing it with its unique spectral signature.

The separation and selectivity of the chemistry in the various regions of OMC-1 is suggestive of a model of the chemistry and structure of molecular clouds in which the cooler and spatially extended halos of these objects contain most of the carbon-rich species while the active cloud cores liberate the more refractory elements depleted onto grains to produce the oxygen-rich molecules also widely observed in dense molecular clouds. Such species appear to be coincident in many clouds because of the weaker velocity structure of most objects and because of the limited spatial resolution that has been used to study them. Thus, while similar mechanisms may also operate in other giant molecular clouds containing embedded sources, due to its proximity and brightness Orion is likely to remain the testing ground upon which much of our knowledge of interstellar chemistry is based.

The authors would like to thank Dave Woody and Steve Scott for their assistance with the extensive observations required to complete the OVRO line survey, and also Dan Watson for many helpful discussions. One of us (G. A. B.) gratefully acknowledges financial support provided by the Miller Research Foundation. Single-dish astronomy at the Owens Valley Observatory is supported by NSF grants AST-8214693 and 8311849.

APPENDIX

ROTATIONAL PARTITION FUNCTIONS

For diatomic and linear molecules the rigid rotor line strengths $S(J)$ and partition functions $Q(T)$ are straightforward, being given by

$$S(J) = J\,, \tag{A1a}$$

$$Q(T) = kT/hB\,, \tag{A1b}$$

in the high-temperature limit, where J is the rotational quantum number of the upper state and B is the rotational constant. The only additional complication is nuclear spin degeneracy. Thus, for example, for HC_3N the above result would be multiplied by a factor of 3 to account for the hyperfine splitting.

The C_{3v} molecules CH_3CN and CH_3CCH have partition functions of

$$Q(T) = \frac{4I^2 + 4I + 1}{4I^2 + 4I + 3}\left[\frac{\pi(kT)^3}{h^3AB^2}\right]^{1/2} = \frac{2}{3}\left[\frac{\pi(kT)^3}{h^3AB^2}\right]^{1/2}, \tag{A2}$$

TABLE 9

DIPOLE MOMENTS USED IN ABUNDANCE CALCULATIONS OF TABLE 1

A.

Species	μ(debye)	Reference
Detected species:		
CN	1.45	1
CO	0.1098	2
CS	1.957	2
NO	0.1587	2
PN	2.743	3
SiO	3.098	2
SO	1.55	2
CCH	0.8	2
HCN	2.984	2
HNC	2.699	2
HCO^+	4.48	4
HCS^+	1.86	5
OCS	0.715	2
HC_3N	3.724	2
NH_3	1.476	2
CH_3CCH	0.75	2
CH_3CN	3.919	2
Upper limits:		
CO^+	2.5	6
PO	1.0	7
C_3N	3.0	8
C_4H	0.9	9
HC_5H	4.330	2

B.

Species	μ_a(debye)	μ_b(debye)	Reference
Detected species			
CH_3OH	0.885	1.440	2
HNCO	1.575	1.35	10
HDO	0.657	1.732	2
H_2S	...	0.974	2
SO_2	...	1.633	2
H_2CO	2.331	...	2
HDCO	2.332	...	11
H_2CS	1.649	...	2
H_2CCO	1.422	...	2
HCOOH	1.396	0.26	2
CH_3CHO	2.55	0.87	2
$HCOOCH_3$	1.63	0.68	12
CH_3OCH_3	...	1.302	13
C_2H_3CN	3.68	1.25	2
C_2H_5CN	3.85	1.23	2
C_3H_2	...	3.3	14
Upper limits:			
HCO	1.3626	0.7	2
CH_3COOH	0.86	1.47	9
C_2H_5OH	0.046	1.438	2
NH_2CHO	3.616	0.852	2
NH_2CH	4.32	...	15
CH_3NH_2	0.304	1.232	16

REFERENCES.—(1) Thomas and Dalby 1968; (2) Poynter and Pickett 1984; (3) Wyse, Manson, and Gordy 1979; (4) Haese and Woods 1979; (5) Gudeman *et al.* 1981; (6) Certain and Woods 1973; (7) assumed value; (8) Wilson and Green 1977; (9) Krisher and Saegebarth 1971; (10) Winnewisser, Hocking, and Gerry 1976; (11) Johns and McKellar 1977; (12) Bauder 1979; (13) Lovas, Lutz, and Dreizler 1979; (14) Thaddeus, Vrtilek, and Gottlieb 1985; (15) Tyler, Sheridan, and Costain 1972; (16) Lide 1952.

the factor of $\frac{2}{3}$ being due to the interchangeable hydrogen nuclei (for which $I = \frac{1}{2}$). This partition function is consistent with the "standard" symmetric top line strength of $S(J, K) = (J^2 - K^2)/J$, where, again, J is the upper state rotational quantum number and K is the projection of J along the C_{3v} symmetry axis. As above, an additional factor of 3 would be needed to account for the hyperfine splitting in CH_3CN.

HDCO, HNCO, HDO, C_2H_3CN, and C_2H_5CN are "standard" asymmetric tops, and therefore have rigid rotor partition functions given by

$$Q(T) = \left[\frac{\pi(kT)^3}{h^3 ABC}\right]^{1/2} . \tag{A3}$$

Hyperfine structure for the later two molecules would involve an additional factor of 3. The molecules H_2CO, H_2CS, H_2CCO, and SO_2 exhibit C_{2v} symmetry, and the presence of interchangeable nuclei modifies the spin-neglected asymmetric top partition function. For H_2CO, H_2CS, and H_2CCO the interchangeable nuclei are spin $\frac{1}{2}$, leading to ortho- and para- forms with spin weights of one and three, respectively. Including both forms, the high-temperature partition function for these species would be

$$Q(T) = 2\left[\frac{\pi(kT)^3}{h^3 ABC}\right]^{1/2} . \tag{A4}$$

For SO_2 the interchangeable oxygen nuclei are spin zero. Half the states are therefore disallowed, and Q becomes

$$Q(T) = \frac{1}{2}\left[\frac{\pi(kT)^3}{h^3 ABC}\right]^{1/2} . \tag{A5}$$

For methanol (CH_3OH) the situation is similar to that of a "standard" asymmetric top, but with the additional complication of internal rotation. The lowest torsional state is split into a singly degenerate A species and a doubly degenerate E species, the nuclear spin weights of which are two and one, respectively. Thus, the total statistical weights of the A and E levels are equal, and in the high-temperature limit one expects the A and E symmetry species to have approximately equal populations, as is observed. This introduces an additional factor of 2 into the usual asymmetric top partition function, that is

$$Q(T) = 2\left[\frac{\pi(kT)^3}{h^3 ABC}\right]^{1/2}$$

Finally, the double internal rotor CH_3OCH_3 has been examined by collapsing the induced splittings and treating the molecule as a rigid asymmetric top without spin, while methyl formate ($HCOOCH_3$) is, theoretically, identical to methanol.

In most cases the low temperatures prevailing in the interstellar medium and the highly energetic nature of most molecular vibrations are such that the vibrational partition function may be safely set to unity. For large, "floppy" molecules like HC_3N, CH_3OH, CH_3OCH_3, or $HCOOCH_3$, however, the lowest energy torsional or bending modes appear at far-infrared wavelengths and can become appreciably populated even at 100–200 K. By assuming that the rotational constants remain the same regardless of vibrational state, the vibrational and rotational partition functions may be factored from each other to give a total partition function $Q_{\rm total}$ of

$$Q_{\rm total}(T) = (1 + \Sigma e^{-h\nu_{\rm vib}/kT}) Q_{\rm rotational}(T) . \tag{A6}$$

We have included such corrections to the total partition function when the neglect of low-lying vibrational states would introduce errors of $\gtrsim 10\%$.

In Table 9 we present a listing of the dipole moments for the detected species along with those of several molecules for which only upper limits have been established. For linear rotors and symmetric tops only a total dipole moment need be given, while for asymmetric tops we list both the A and B inertial axis values where appropriate.

REFERENCES

Allen, M., and Robinson, G. W. 1977, *Ap. J.*, **212**, 396.
Barlow, S. E., Dunn, G. H., and Schauer, M. 1984, *Phys. Rev. Letters*, **52**, 902.
Bastien, P., Bieging, J., Henkel, C., Martin, R. N., Pauls, T., Walmsley, C. M., and Ziurys, L. M. 1981, *Astr. Ap.*, **98**, L4.
Bauder, A. 1979, *J. Phys. Chem. Ref. Data*, **8**, 583.
Becklin, E. E., and Neugebauer, G. 1967, *Ap. J.*, **147**, 799.
Blake, G. A., Sutton, E. C., Masson, C. R., and Phillips, T. G. 1986, *Ap. J. Suppl.*, **60**, 357.
Blake, G. A., Sutton, E. C., Masson, C. R., Phillips, T. G., Herbst, E., Plummer, G. M., and De Lucia, F. C. 1984, *Ap. J.*, **286**, 586.
Boland, W., de Graauw, T., Lidholm, S., and Lee, T. J. 1983, *Ap. J.*, **271**, 183.
Boland, W., and de Jong, T. 1982, *Ap. J.*, **261**, 110.
Certain, P. R., and Woods, R. C. 1973, *J. Chem. Phys.*, **58**, 5837.
Cohen, R. S., Cong, H., Dame, T. M., and Thaddeus, P. 1980, *Ap. J* (*Letters*), **239**, L53.
Cummins, S. E., Linke, R. A., and Thaddeus, P. 1986, *Ap. J. Suppl.*, **60**, 819.
Dalgarno, A. 1982, *Phil. Trans. Roy. Soc. London*, *A*, **303**, 513.
d'Hendecourt, L. B., Allamandola, L. J., Baas, F., and Greenberg, J. M. 1982, *Astr. Ap.*, **109**, L12.
Elias, J. H., *et al.* 1978, *Ap. J.*, **220**, 25.
Frerking, M. A., Keene, J., Blake, G. A., Phillips, T. G., and Beichman, C. A. 1986, *Ap. J.*, submitted.
Gautier, T. N., III, Fink, U., Treffers, R. R., and Larson, H. P. 1976, *Ap. J.* (*Letters*), **207**, L129.
Genzel, R., Downes, D., Ho, P. T. P., and Bieging, J. 1982, *Ap. J.* (*Letters*), **259**, L103.
Genzel, R., Reid, M. J., Moran, J. M., and Downes, D. 1981, *Ap. J.*, **244**, 884.
Glassgold, A. E., Huggins, P. J., and Langer, W. D. 1985, *Ap. J.*, **290**, 615.
Goldsmith, P. F., Krotkov, R., Snell, R. L., Brown, R. D., and Godfrey, P. 1983, *Ap. J.*, **274**, 184.
Goldsmith, P. F., and Linke, R. A. 1981, *Ap. J.*, **245**, 482.
Gudeman, C. S., Haese, N. N., Piltch, N. P., and Woods, R. C. 1981, *Ap. J.* (*Letters*), **246**, L47.
Haese, N. N., and Woods, R. C. 1979, *Chem. Phys. Letters*, **61**, 396.
Hall, D. N. B. 1984, *Galactic and Extragalactic Infrared Spectroscopy*, ed. M. F. Kessler and J. P. Phillips (Dordrecht: Reidel), p. 267.
Hartquist, T. W., Oppenheimer, M., and Dalgarno, A. 1980, *Ap. J.*, **236**, 182.
Hasegawa, T. 1986, *Ap. Space Sci.*, **118**, 421.
Hasegawa, T., *et al.* 1984, *Ap. J.*, **283**, 117.
Herbst, E. 1983, *Ap. J. Suppl.*, **53**, 41.

Herbst, E. 1985, *Ap. J.*, **291**, 226.
———. 1986, *Ap. J.*, **306**, 667.
Herbst, E., Adams, N. G., and Smith, D. 1983, *Ap. J.*, **269**, 329.
Herbst, E., and Klemperer, W. 1973, *Ap. J.*, **185**, 505.
Herbst, E., and Leung, C. M. 1986, *Ap. J.*, **310**, 378.
Hermsen, W., Wilson, T. L., Walmsley, C. M., and Batrla, W. 1985, *Astr. Ap.*, **146**, 134.
Huggins, P. J., Carlson, W. J., and Kinney, A. L. 1984, *Astr. Ap.*, **133**, 347.
Huntress, W. T., Jr. 1977, *Ap. J. Suppl.*, **33**, 495.
Huntress, W. T., Jr., and Mitchell, G. F. 1979, *Ap. J.*, **231**, 456.
Iglesias, E. R., and Silk, J. 1978, *Ap. J.*, **226**, 851.
Irvine, W. M., and Hjalmarson, A. 1984, *Origins of Life* (Dordrecht: Reidel).
Irvine, W. M., Schloerb, F. P., Hjalmarson, A., and Herbst, E. 1985, *Protostars and Planets*, Vol. 2 (Tucson: University of Arizona Press).
Johansson, L. E. B., *et al.* 1984, *Astr. Ap.*, **130**, 227.
Johns, J. W. C., and McKellar, A. R. W. 1977, *J. Molec. Spectrosc.*, **64**, 327.
Johnston, K. J., Palmer, P., Wilson, T. L., and Bieging, J. H. 1983, *Ap. J. (Letters)*, **271**, L89.
Jones, A. P., and Williams, D. A. 1984, *M.N.R.A.S.*, **209**, 955.
Keene, J., Blake, G. A., and Phillips, T. G. 1983, *Ap. J. (Letters)*, **271**, L27.
Keene, J., Blake, G. A., Phillips, T. G., Huggins, P. J., and Beichman, C. A. 1985, *Ap. J.*, **299**, 967.
Kleinmann, D. W., and Low, F. J. 1967, *Ap. J. (Letters)*, **149**, L1.
Knacke, R. F., McCorkle, S., Puetter, R. C., Erickson, E. F., and Kratschmer, W. 1982, *Ap. J.*, **260**, 141.
Krisher, L. C., and Saegebarth, E. 1971, *J. Chem. Phys.*, **54**, 4553.
Krolik, J. H., and Kallman, T. R. 1983, *Ap. J.*, **267**, 610.
Kuiper, T. B. H., Zuckerman, B., and Rodriguez-Kuiper, E. N. 1981, *Ap. J.*, **251**, 88.
Kutner, M. L., Tucker, K. D., Chin, G., and Thaddeus, P. 1977, *Ap. J.*, **215**, 521.
Langer, W. D., Graedel, T. E., Frerking, M. A., and Armentrout, P. B. 1984, *Ap. J.*, **277**, 581.
Leger, A., Jura, M., and Omont, A. 1985, *Astr. Ap.*, **144**, 147.
Leung, C. M., Herbst, E., and Huebner, W. F. 1984, *Ap. J. Suppl.*, **56**, 231.
Lide, D. R. 1952, *J. Chem. Phys.*, **20**, 1812.
Linke, R. A., Frerking, M. A., and Thaddeus, P. 1978, *Ap. J. (Letters)*, **234**, L139.
Linke, R. A., Guélin, M., and Langer, W. D. 1983, *Ap. J. (Letters)*, **271**, L85.
Liszt, H. S., Wilson, R. W., Penzias, A. A., Jefferts, K. B., Wannier, P. G., and Solomon, P. M. 1974, *Ap. J.*, **190**, 557.
Lovas, F. J., Lutz, J., and Dreizler, H. 1979, *J. Phys. Chem. Ref. Data*, **8**, 1051.
Masson, C. R., *et al.* 1984, *Ap. J. (Letters)*, **283**, L37.
Masson, C. R., Claussen, M. J., Lo, K. Y., Moffet, A. T., Phillips, T. G., Sargent, A. I., Scott, S. L., and Scoville, N. Z. 1985, *Ap. J. (Letters)*, **295**, L47.
Matsakis, D. N., Cheung, A. C., Wright, M. C. H., Askne, J. I. H., Townes, C. H., and Welch, W. J. 1980, *Ap. J.*, **236**, 481.
Morris, M., Palmer, P., and Zuckerman, B. 1980, *Ap. J.*, **237**, 1.
Mundy, L., Scoville, N. Z., Baath, L. B., Masson, C. R., and Woody, D. W. 1986, *Ap. J. (Letters)*, **304**, L51.
Olofsson, H. 1984, *Astr. Ap.*, **134**, 36.
Penzias, A. A. 1981, *Ap. J.*, **249**, 513.
Phillips, T. G., Blake, G. A., Keene, J., Woods, R. C., and Churchwell, E. 1985, *Ap. J. (Letters)*, **294**, L45.
Phillips, T. G., and Huggins, P. J. 1981, *Ap. J.* **251**, 533.
Phillips, T. G., Huggins, P. J., Kuiper, T. B. H., and Miller, R. E. 1980, *Ap. J. (Letters)*, **238**, L103.
Phillips, T. G., Kwan, J., and Huggins, P. J. 1980, in *IAU Symposium 87, Interstellar Molecules*, ed. B. Andrews (Dordrecht: Reidel), p. 21.
Plambeck, R. L., Wright, M. C. H., Welch, W. J., Bieging, J. H., Baud, B., Ho, P. T. P., and Vogel, S. N. 1982, *Ap. J.*, **259**, 617.
Poynter, R. L., and Pickett, H. M. 1984, *Submillimeter, Millimeter, and Microwave Spectral Line Catalogue* (JPL Pub. 80-23, Rev. 2).
Prasad, S. S., and Huntress, W. T., Jr. 1980, *Ap. J. Suppl.*, **43**, 1.
———. 1982, *Ap. J.*, **260**, 590.
Prasad, S. S., and Tarafdar, S. P. 1983, *Ap. J.*, **267**, 603.
Schloerb, F. P., Friberg, P., Hjalmarson, A., Hoglund, B., and Irvine, W. M. 1983, *Ap. J.*, **264**, 161.
Scoville, N. Z., Kleinmann, S. G., Hall, D. N. B., and Ridgway, S. T. 1983, *Ap. J.*, **275**, 201.
Snell, R. L., Mundy, L. G., Goldsmith, P. F., Evans, N. J., and Erickson, N. R. 1984, *Ap. J.*, **276**, 625.
Sutton, E. C., Blake, G. A., Genzel, R., Masson, C. R., and Phillips, T. G. 1986, *Ap. J.*, **311**, 921.
Sutton, E. C., Blake, G. A., Masson, C. R., and Phillips, T. G. 1984, *Ap. J. (Letters)*, **283**, L41.
———. 1985, *Ap. J. Suppl.*, **58**, 341.
Sweitzer, J. S. 1978, *Ap. J.*, **225**, 116.
Tarafdar, S. P., Prasad, S. S., Huntress, W. T., Villere, K. R., and Black, D. C. 1985, *Ap. J.*, **289**, 220.
Thaddeus, P., Kutner, M. L., Penzias, A. A., Wilson, R. W., and Jefferts, K. B. 1972, *Ap. J. (Letters)*, **176**, L73.
Thaddeus, P., Vrtilek, J. M., and Gottlieb, C. A. 1985, *Ap. J. (Letters)*, **299**, L63.
Thomas, R., and Dalby, F. W. 1968, *Canadian J. Phys.*, **46**, 2815.
Tielens, A. G. G. M., and Hagen, W. 1982, *Astr. Ap.*, **114**, 245.
Townes, C. H., and Schawlow, A. L. 1955, *Microwave Spectroscopy* (New York: Dover).
Tyler, J. K., Sheridan, J., and Costain, C. C. 1972, *J. Molec. Spectrosc.*, **43**, 248.
Vogel, S. N., Bieging, J. H., Plambeck, R. L., Welch, W. J., and Wright, M. C. H. 1985, *Ap. J.*, **290**, 600.
Wannier, P. G., Linke, R. A., and Penzias, A. A. 1981, *Ap. J.*, **247**, 522.
Wannier, P. G., Penzias, A. A., and Jenkins, E. B. 1982, *Ap. J.*, **254**, 100.
Watson, D. M. 1982, Ph.D. thesis, University of California, Berkeley.
Watson, D. M., Genzel, R., Townes, C. H., and Storey, J. W. V. 1985, *Ap. J.*, **298**, 316.
Watson, D. M., Storey, J. W. V., Townes, C. H., Haller, E. E., and Hansen, W. L. 1980, *Ap. J. (Letters)*, **239**, L129.
Watt, G. D. 1985, *M.N.R.A.S.*, **212**, 93.
Werner, M. W., Crawford, M. K., Genzel, R., Hollenbach, D. J., Townes, C. H., and Watson, D. M. 1984, *Ap. J. (Letters)*, **282**, L81.
Werner, M. W., Dinerstein, H. L., and Capps, R. W. 1983, *Ap. J. (Letters)*, **265**, L13.
Westbrook, W. E., Werner, M. W., Elias, J. H., Gezari, D. Y., Hauser, M. G., Lo, K. Y., and Neugebauer, G. 1976, *Ap. J.*, **209**, 94.
Whittet, D. C. B., Bode, M. F., Longmore, A. J., Baines, D. W. T., and Evans, A. 1983, *Nature*, **303**, 218.
Williams, D. A., and Hartquist, T. W. 1984, *M.N.R.A.S.*, **210**, 141.
Wilson, S., and Green, S. 1977, *Ap. J. (Letters)*, **212**, L87.
Wilson, R. W., Jefferts, K. B., and Penzias, A. A. 1970, *Ap. J. (Letters)*, **161**, L43.
Wilson, T. L., Serabyn, E., Henkel, C., and Walmsley, C. M. 1986, *Astr. Ap.*, **158**, L1.
Winnewisser, G., Hocking, W. H., and Gerry, M. C. L. 1976, *J. Phys. Chem. Ref. Data*, **5**, 79.
Wootten, A., Bozyan, E. P., Garrett, D. B., Loren, R. B., and Snell, R. L. 1980, *Ap. J.*, **239**, 844.
Wootten, A., Evans, N. J., Snell, R., and Vanden Bout, P. 1978, *Ap. J. (Letters)*, **225**, L143.
Wootten, A., Loren, R. B., and Bally, J. 1984, *Ap. J.*, **277**, 189.
Wootten, A., Snell, R., and Evans, N. J. 1980 *Ap. J.*, **240**, 532.
Wright, M. C. H., and Plambeck, R. L. 1983, *Ap. J. (Letters)*, **267**, L115.
Wright, M. C. H., Plambeck, R. L., Vogel, S. N., Ho, P. T. P., and Welch, W. J. 1983, *Ap. J. (Letters)*, **267**, L41.
Wright, M. C. H., and Vogel, S. N. 1985, *Ap. J. (Letters)*, **297**, L11.
Wynn-Williams, C. G., Genzel, R., Becklin, E. E., and Downes, D. 1984, *Ap. J.*, **281**, 172.
Wyse, F. C., Manson, E. L., and Gordy, W. 1972, *J. Chem. Phys.*, **57**, 1106.
Zuckerman, B., Kuiper, T. B. H., and Rodriguez-Kuiper, E. N. 1976, *Ap. J. (Letters)*, **209**, L137.

GEOFFREY A. BLAKE and E. C. SUTTON: Space Sciences Laboratory, University of California, Berkeley, CA 94720

C. R. MASSON: Downes Laboratory of Physics 405-47, California Institute of Technology, Pasadena, CA 91125

T. G. PHILLIPS: Downes Laboratory of Physics 320-47, California Institute of Technology, Pasadena, CA 91125